

Review

# Graphene Quantum Dots-Based Nanocomposites Applied in Electrochemical Sensors: A Recent Survey

Murilo H. M. Facure <sup>1,2</sup>, Rodrigo Schneider <sup>1,2</sup>, Jessica B. S. Lima <sup>3</sup>, Luiza A. Mercante <sup>3</sup>  
and Daniel S. Correa <sup>1,2,\*</sup>

- <sup>1</sup> Nanotechnology National Laboratory for Agriculture (LNNA), Embrapa Instrumentação, São Carlos 13561-206, Brazil; mfacure@estudante.ufscar.br (M.H.M.F.); rodrigoss@estudante.ufscar.br (R.S.)  
<sup>2</sup> PPGQ, Department of Chemistry, Center for Exact Sciences and Technology, Federal University of São Carlos (UFSCar), São Carlos 13565-905, Brazil  
<sup>3</sup> Institute of Chemistry, Federal University of Bahia (UFBA), Salvador 40170-110, Brazil; jessicabs@ufba.br (J.B.S.L.); lmercante@ufba.br (L.A.M.)  
\* Correspondence: daniel.correa@embrapa.br

**Abstract:** Graphene quantum dots (GQDs) have been widely investigated in recent years due to their outstanding physicochemical properties. Their remarkable characteristics allied to their capability of being easily synthesized and combined with other materials have allowed their use as electrochemical sensing platforms. In this work, we survey recent applications of GQDs-based nanocomposites in electrochemical sensors and biosensors. Firstly, the main characteristics and synthesis methods of GQDs are addressed. Next, the strategies generally used to obtain the GQDs nanocomposites are discussed. Emphasis is given on the applications of GQDs combined with distinct 0D, 1D, 2D nanomaterials, metal-organic frameworks (MOFs), molecularly imprinted polymers (MIPs), ionic liquids, as well as other types of materials, in varied electrochemical sensors and biosensors for detecting analytes of environmental, medical, and agricultural interest. We also discuss the current trends and challenges towards real applications of GQDs in electrochemical sensors.

**Keywords:** graphene quantum dots; GQDs; nanocomposites; electrochemical sensors; nanomaterials



**Citation:** Facure, M.H.M.; Schneider, R.; Lima, J.B.S.; Mercante, L.A.; Correa, D.S. Graphene Quantum Dots-Based Nanocomposites Applied in Electrochemical Sensors: A Recent Survey. *Electrochem* **2021**, *2*, 490–519. <https://doi.org/10.3390/electrochem2030032>

Academic Editor: Masato Sone

Received: 26 June 2021

Accepted: 1 September 2021

Published: 6 September 2021

**Publisher's Note:** MDPI stays neutral with regard to jurisdictional claims in published maps and institutional affiliations.



**Copyright:** © 2021 by the authors. Licensee MDPI, Basel, Switzerland. This article is an open access article distributed under the terms and conditions of the Creative Commons Attribution (CC BY) license (<https://creativecommons.org/licenses/by/4.0/>).

## 1. Introduction

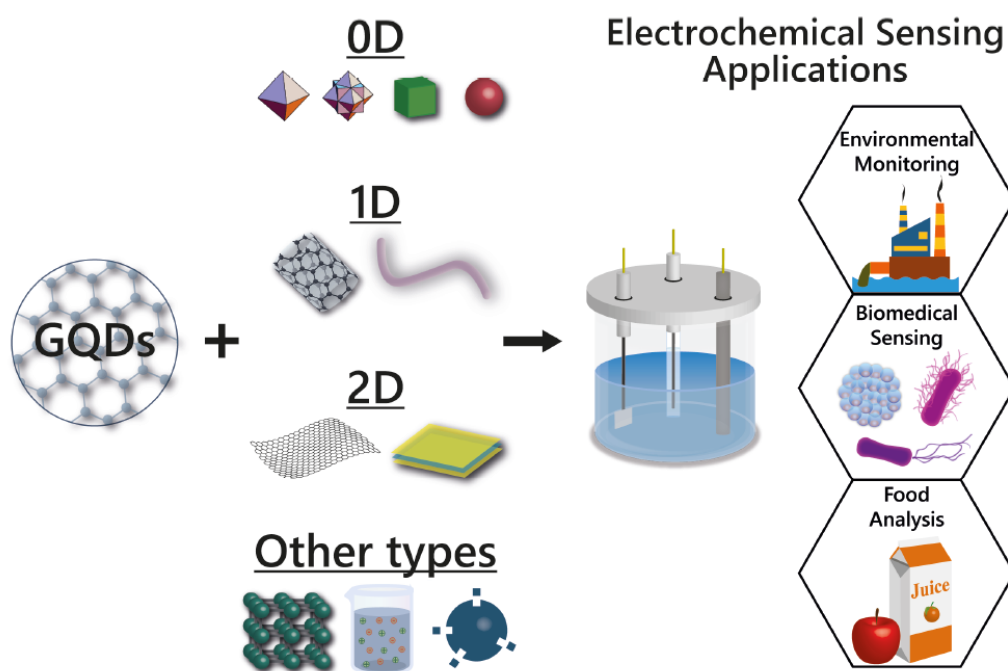
The discovery of graphene [1,2] has generated enormous interest in graphene-based materials [3–6], including in graphene quantum dots (GQDs) [7], owing to their appealing features, which include ease of production and remarkable physical-chemical properties [8–11]. GQDs present the carbon structure of graphene, i.e., carbon atoms organized in hexagonal rings, but with lateral dimensions inferior to 100 nm. Since they present less than 10 atomic layers and all the dimensions are within the nanoscale, GQDs are considered 0D materials [12]. Due to the quantum confinement and edge effects resulting from the modification of the electron distribution, GQDs present a bandgap responsible for their luminescent properties and changes in their electrical conductivity [8,13], which can be tuned according to the GQDs size and structure [14–16].

GQDs have also been successfully employed in electrochemical sensors [17–19], which make use of redox reactions and other charge-transfer phenomena to detect and quantify a target analyte [20,21]. Recent research on electrochemical sensors has been primarily dedicated to improve the sensing performance in terms of detection limits, linear dynamic ranges, sensitivities, electrode fouling conditions, response times, and over-potential issues. In this direction, the materials employed in electrodes are key for designing high-performance electrochemical sensors [22,23], with emphasis on nanomaterials, which can improve sensor's sensitivity or selectivity based on their strong electrochemical properties [20,24]. In this regard, the outstanding performance of the sensors using GQDs-based materials can be mainly attributed to their large surface-to-volume ratio as well as to

their multiple molecule recognition sites. The interaction with the target analyte can be performed in the edge sites, through functionalized groups, or via  $\pi$ - $\pi$  interaction [8,25,26]. Furthermore, the charge transfer of GQDs can be modulated according to the intended application. In general, the removal of the functional groups leads to GQDs with a more pronounced  $sp^2$  hybridization character, which results in an electrical resistance decrease. However, the maintenance of such functional groups can assist in the interaction with analytes, which is a fundamental condition for sensing applications. In this direction, many papers have reported the increase in charge transfer when using GQDs in electrochemical applications, even using functionalized ones. Such a behavior can be explained in terms of the  $sp^2$  carbon islands that remain in the functionalized GQDs and facilitates the charge transfer [9,27].

GQDs also present electrochemiluminescence (ECL), a property that is key for developing sensors. In this sort of application, GQDs are excited by an electric potential and the produced excited state emits light when deactivated, which can be measured and used in the analyte quantification [28,29]. GQDs can also be considered as nanozymes, i.e., they can mimic enzyme activities [30,31], sometimes with performance superior to that of the natural enzymes [32–37].

The use of GQDs in electrochemistry is also preferred favored by their ease of production and the possibility to be doped or modified aiming at specific sensing applications [38–40]. These characteristics enable GQDs-based nanomaterials to have lower detection limits and higher sensitivities. In many cases, they can also be combined with other materials to produce GQDs-based nanocomposites with the aim of creating synergetic effects to facilitate catalytic reactions with target analytes [8,12,17,41–43]. In this regard, this review surveys the most prominent applications of GQDs-based nanocomposites in electrochemical sensors. Firstly, the syntheses' methods to produce GQDs are briefly presented, followed by the strategies generally used to obtain GQDs-based nanocomposites. Then, the physical and chemical properties of GQDs are addressed. Next, we review important results on GQDs-based nanocomposites applied in electrochemical sensing by specifically considering the dimensionalities of the material combined with the GQDs, as illustrated in Scheme 1. Finally, perspectives on the use of GQDs-based nanocomposites in electrochemical sensing applications are presented.



**Scheme 1.** Schematic illustration of GQDs combined with different materials to be used in electrochemical sensing applications.

## 2. Graphene Quantum Dots Synthesis

The syntheses employed to produce GQDs have a direct effect on their structures and properties, and consequently on their sensing performance for varied applications. GQDs can be obtained through top-down or bottom-up routes, as illustrated in Figure 1. The parameters used in each route can be modified to provide GQDs with desired characteristics. As there are many reviews available in the literature addressing GQDs synthesis procedures [11,38–41,44,45], herein we will only briefly cover the main approaches to obtain GQDs and their modification through doping and functionalization. In this sense, in the next topic, we emphasize the techniques generally used to combine other materials with GQDs.

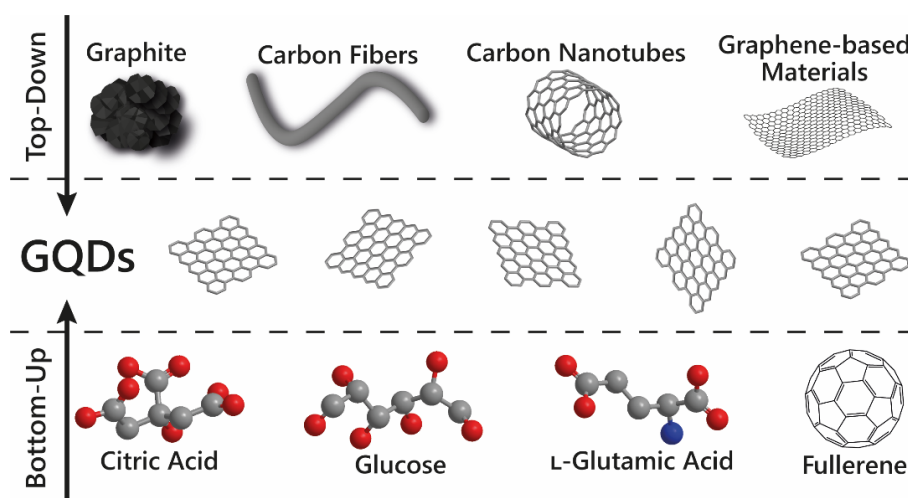


**Figure 1.** Top-down and bottom-up routes employed to synthesize GQDs.

### 2.1. Top-Down

Top-down synthesis consists of cleaving or cutting down carbon-based materials with a graphitic structure to obtain GQDs. The most used precursors are graphene and graphene-based materials [46,47], graphite [48], carbon nanotubes (CNTs) [49], and carbon fibers [50,51]. Physical, chemical, or electrochemical approaches can be used to reduce the size of the precursors. Hydrothermal and solvothermal syntheses are the most employed methods to produce GQDs using top-down routes. In addition, chemical or electrochemical exfoliation and cutting methods [52–55], microwave and ultrasonic syntheses [56–59], photo-Fenton reactions [60], and lithography [61] are some other methods usually employed [8,11,18]. As the main disadvantage, top-down methods do not enable the precise control of the GQDs morphology and size, and generally, give rise to GQDs with surface defects. Moreover, some routes usually require the use of laborious and multistep procedures and the need for using strong acid reactants and high temperatures [11,25,27].

### 2.2. Bottom-Up

Bottom-up synthesis uses small and aromatic molecules (e.g., citric acid [62,63], L-glutamic acid [64], glucose [65,66], and polycyclic aromatic hydrocarbon molecules [67]), or nanoclusters in controlled processes to prepare high-quality GQDs. Pyrolysis of organic precursors, decomposition of fullerene [68,69], chemical vapor deposition [70,71], and step-by-step organic synthesis are some examples of bottom-up methods used to produce GQDs [11,25]. In general, better control of the size, morphology, shape, and surface state can be achieved with bottom-up approaches. On the other hand, good control of the experimental conditions is required to achieve the high quality intended [8,18,25].

### 2.3. GQDs Doping and Functionalization

GQDs are rarely used in their pristine form. GQDs are usually obtained with functionalized oxygen-containing groups, and other functionalization can be further performed to render the desired characteristics. For instance, doping GQDs with heteroatoms, specific molecules, enzymes, nanoparticles, DNA strands, and enzymes have already been reported [8,12,39]. These modifications can be performed in the precursor (pre-modification), giving rise to functionalized GQDs, or after GQDs synthesis (post-modification). Covalent and noncovalent functionalization can be employed at the core or the edges of the nanoparticles. The first type occurs through chemical bonds and leads to changes in the hybridization of the C atoms. In contrast, noncovalent modifications are performed through  $\pi$ - $\pi$  and intermolecular interactions and preserve the  $\pi$ -conjugation of the GQDs' core [8,12,25].

## 3. Strategies for Producing GQDs-Based Nanocomposites

### 3.1. Electrodeposition

Electrodeposition is a controlled process in which the nanomaterial is deposited onto the surface of a conductive substrate by applying an electrical potential in a solution containing ions [72,73]. The method can be performed employing different electrochemical techniques and enables the precise control of the deposited material by controlling the applied potential and deposition time, combined with low cost. Moreover, the technique does not require the use of binding agents, chemical reductants/oxidants, or stabilizers, and does not generate by-products. [72,74]. The electrodeposition has been widely applied to obtain metallic nanoparticles. In the underpotential deposition process, a metal cation present on the electrolyte is chemically reduced to a metal solid at the electrode surface [4,75,76]. Besides 0D nanomaterials, the technique is also used to deposit 1D and 2D nanostructures, using conductive polymers, carbon-based materials, layered double hydroxides (LDH), and other inorganic materials [74]. As GQDs can also be electrodeposited, the GQD-based nanocomposite fabrication can be easily performed using electrodeposition techniques. In this way, the obtained modified electrode is ready to be used in the electrochemical sensing application [77–79].

### 3.2. Electrospinning

Electrospinning is a technique in which fibers having diameters ranging from nano- to micrometers are produced by the application of electrical forces on a droplet of a polymer solution that is elongated to form the fibers [80–82]. As the main advantages of electrospinning, one can cite the versatility in the materials employed to produce the fibers, the fast production of 1D structures, and the high surface-area-to-volume ratio obtained, enabling the nanofibers' modification with other materials [83–85]. The combination with GQDs can be performed before or after the fiber synthesis. In the first case, GQDs can be added to the solution to be electrospun, while the post-modification can be performed by drop-casting the solution material onto the nanofibers, by dip-coating the fiber membrane in the GQDs solution, or by self-assembly strategies [86–89].

### 3.3. Hydrothermal/Solvothermal Synthesis

Hydro- and solvothermal syntheses are widely used to produce GQDs, taking advantage of both bottom-up and top-down approaches. These syntheses make use of soluble or insoluble materials in an aqueous solution or organic solvent in a sealed and heated reactor, such as an autoclave. In the syntheses, a relatively high temperature (100–1000 °C) and high pressure (1–100 MPa) reaction environment is created through heating. The regulation of the synthesized material properties can frequently be performed by changing the synthesis parameters [90,91]. The hydrothermal/solvothermal approaches also allow the fabrication of GQDs-based nanocomposites in a one-step procedure, in which the GQDs precursor and the other material to be combined with are reacted together in the autoclave. The resulting dispersion can be directly used to modify the electrode for electrochemical applications.

Otherwise, the dispersion can be subjected to purification and separation processes, such as filtration, centrifugation, and dialysis to obtain the isolated nanocomposite [55,92–96].

### 3.4. Co-Precipitation Method

Another strategy that can be used to obtain GQDs-based nanocomposites is the co-precipitation method. In this approach, the starting materials present in the solution are collected as a solid after the addition of a precipitating agent, the acquisition of a supersaturated solution, or by any process capable to induce the precipitation of the materials [97,98]. This method is generally used to obtain GQDs combined with inorganic nanoparticles. In this case, metal salts are used as precursors to obtain the nanoparticles in the presence of pre-synthesized GQDs [99,100]. In this process, nucleation is key to determine the amount and size of the as-obtained nanoparticles [97].

### 3.5. Other Strategies

In addition to the previously mentioned strategies, the combination of different materials can be performed using more direct methods by separately obtaining GQDs and the materials to be combined. In this way, the materials can be mixed in a unique solution, and techniques such as drop-casting [101,102] and spin-coating [103,104] can be used to modify the electrodes. If they are in separated solutions, self-assembly techniques can be employed, such as layer-by-layer [105–107] and dip-coating [108,109].

## 4. Physicochemical Characterization of GQDs

As previously mentioned, many other review works have extensively covered the physicochemical properties of GQDs [8,9,11,12,25–27,40,41,44]. For this reason, in this section, we briefly address the most used characterization techniques. In addition, in the next section, we highlight the effect of the size and edges on the electrochemical sensing performance of the GQDs.

UV-vis spectroscopy technique is routinely used for GQDs and carbon-based materials characterization due to its simplicity, low cost, and fast analysis. In the case of the GQDs, UV-vis spectroscopy allows the observation of two electronic transitions, namely the  $\pi$ - $\pi^*$  and  $n$ - $\pi^*$  [110]. The peak related to the  $\pi$ - $\pi^*$  transition is located between 230 nm and 270 nm, which is ascribed to C=C bonds of the aromatic carbon skeleton, i.e., to the  $sp^2$  hybridized carbon atoms. The  $n$ - $\pi^*$  transition appears as a shoulder at around 290–330 nm, and it is mainly attributed to oxygen moieties or defects present in the GQDs [8]. Interestingly, the functionalization/modifications in GQDs structure can be investigated by changes in the intensity of this shoulder at 290–330 nm [111,112]. Additionally, another shoulder above 390 nm may be observed in the spectra under certain synthetic conditions, revealing surface states ascribed to defects introduced by groups moieties in the GQDs structure (Figure 2A) [113].

Fourier-transform infrared spectroscopy (FTIR) enables the identification of some chemical bonds (C=C, C-O, C-OH, C=O) in the vibrational absorption spectra of GQDs in a fast and non-destructive way [8,114]. An interesting study by Chhabra and co-workers demonstrated that the FTIR spectroscopy was useful to analyze GQDs and displaying different functional groups that rendered them with different emissions colors at the indigo, blue, green, yellow, and red regions (Figure 2B) [115].

Raman spectroscopy analysis of GQDs is mainly studied in terms of the D ( $\approx 1580\text{ cm}^{-1}$ ) and the G ( $\approx 1350\text{ cm}^{-1}$ ) characteristic modes of graphitic materials [55,116]. The D band originates from the GQDs edge states or the defects in the GQDs structure. The G band originates from the in-plane C=C stretching. In this way, the  $I_D/I_G$  ratio is generally used to analyze the amount of functionalized groups in the GQDs structure [117,118]. Additionally, there are others GQDs Raman modes, viz. the 2D ( $\approx$ at  $2650\text{ cm}^{-1}$ ), D + G ( $\approx$ at  $2900\text{ cm}^{-1}$ ), and 2G ( $\approx$ at  $3187\text{ cm}^{-1}$ ) peaks (Figure 2C) [118].

X-ray photoelectron spectroscopy (XPS) (Figure 2D) is used to evaluate the atomic composition of the GQDs, as well as can provide information about the functionalized

groups present on their structure and their oxidation degree [88,119–121]. The main advantages of the XPS include the determination of the doping content and the degree of reduction of GQDs. [120]. Furthermore, it can be used to understand shifts in the PL emission spectra [119].

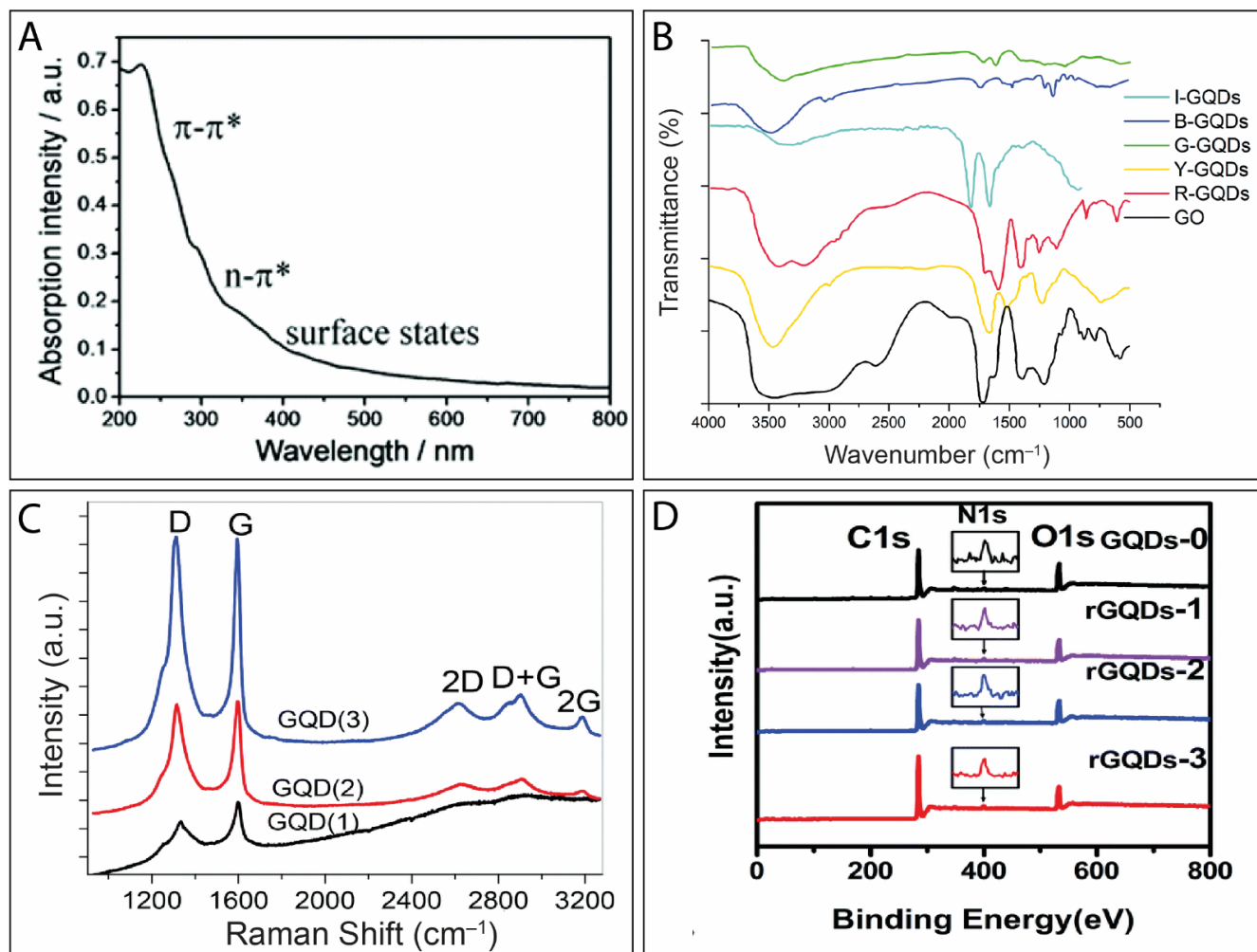


**Figure 2.** (A) A typical UV-vis absorption spectrum of GQDs. Reproduced with permission from reference [113]. Copyright 2018 The Royal Society of Chemistry. (B) FTIR spectra of GQDs samples. I-GQDs (Indigo emitting), B-GQDs (Blue emitting), G-GQDs (Green emitting), Y-GQDs (Yellow emitting), R-GQDs (Red emitting), and GO (Graphene Oxide). Reproduced with permission from reference [115]. Copyright 2018 The Royal Society of Chemistry. (C) Raman spectra of three different samples of GQD. Reproduced with permission of reference [118]. Copyright 2018 The Royal Society of Chemistry. (D) XPS spectra of GQDs with different reduced levels. Reproduced with permission of reference [120]. Copyright 2019 The Royal Society of Chemistry.

Photoluminescence (PL) spectroscopy is frequently employed for GQDs characterization as well as for their sensing performance evaluation. GQDs usually present emission dependence from the excitation wavenumber due to the presence of different functional groups on their structures [122]. Moreover, the technique can provide information about the material's bandgap and can be used to estimate the GQDs quantum yield (QY) [8,121,123,124]. Zhu et al. suggested that in graphene oxide quantum dots (GOQDs), the PL originates from the surface defects, i.e., the oxygen-containing groups bonded to the surface (defect state emission), while for their reduced form (rGOQDs), the PL originates from electron-hole recombination or size and zigzag edge effects (intrinsic state emission) (Figure 3A) [121].

X-ray diffraction (XRD) analysis provides information about the crystallinity and spacing between the few layers of GQDs. For instance, the exfoliation of graphite and the confirmation of the GQDs synthesis can be monitored using XRD. Graphite presents a sharp peak at  $2\theta \approx 26^\circ$ , while GQDs present a broader and weaker peak in the same region (Figure 3B). However, this peak can be shifted due to the presence of functional groups on the GQDs' structure [48,125].

Transmission electron microscopy (TEM) is employed to observe morphological aspects of GQDs at atomic level, such as local defects, thickness, orientation, and lattice structure (Figure 3C) [126]. The high-resolution TEM (HRTEM) allows the investigation of the lattice fringe structure and the determination of the interlayer and in-plane lattice spacing. For GQDs, this value is close to 0.24 nm [127,128]. Other microscopy techniques are also employed for GQDs characterization. For instance, Ritter and Lyding characterized GQD nanostructures employing high-resolution scanning tunneling microscopy (STM) with atomic resolution to obtain topographical images [129]. According to the authors, the STM technique associated with scanning tunneling spectroscopy (STS) allowed the determination of the crystallographic orientation of the edges and enabled the differentiation of zigzag and armchair types. The STS provided a zigzag ratio of 0.65 nm and 0.44 nm of the GQDs, as shown in Figure 3D. Atomic force microscopy (AFM) (Figure 3E(i)) is widely employed to evaluate the height of the GQD particles and consequently the number of stacked layers (Figure 3E(ii)) [45,55,130].

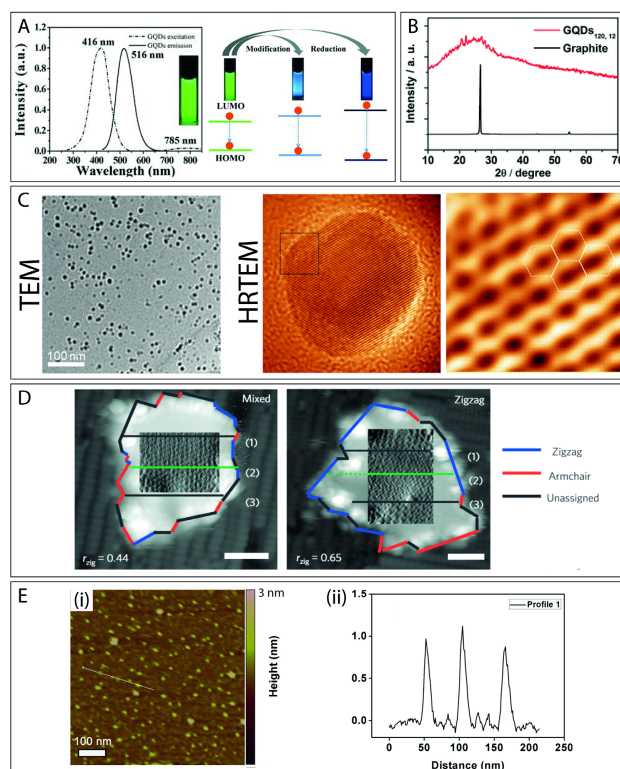


**Figure 3.** (A) Excitation (dashed line) and emission (solid line) photoluminescence spectra of GQDs and a schematic illustration of the bandgap changing of GQDs with different surface defects. Reproduced with permission from reference [121]. Copyright 2012 Wiley. (B) XRD patterns of graphite and GQDs<sub>120,12</sub> (obtained at 120 °C in a 12 h synthesis). Adapted with permission from reference [48]. Copyright 2013 The Royal Society of Chemistry. (C) TEM images for GOQDs and HRTEM images of single GOQDs. Reproduced with permission from reference [126]. Copyrights 2020 Wiley. (D) Determination of the edge types of the GQDs by STM analysis. The values of 0.65 and 0.44 are ascribed to the fraction of zigzag edges. Scale bars = 2 nm. Reproduced with permission from reference [129]. Copyright 2009 Nature. (E) (i) AFM images of GQDs and (ii) the resulted height profile of the GQDs. Reproduced with permission from reference [130]. Copyright 2017 Elsevier.

## 5. Electrochemical Performance of GQDs

Several electrochemical techniques can be employed to investigate the electrochemical behavior of GQDs, including cyclic voltammetry (CV), galvanostatic charge–discharge curves, amperometry, differential pulse voltammetry (DPV), and electrochemical impedance spectroscopy (EIS), among others. To perform such measurements, GQDs are deposited on the working electrode using the techniques mentioned in Section 3. Many works have reported excellent performances of GQDs in electrochemical applications, leading to enhancements in current densities and sensor devices with greater sensitivity [131–133]. Specifically, the edge types and size of the GQDs have been reported to play a fundamental role in such electrochemical applications. In this context, we evaluate the effects provided by these features in the GQDs final electrochemical properties in this section.

### 5.1. Effect of the Edges of GQDs on Their Electrochemical Performance

GQDs can present armchair edges, zigzag edges, or a combination of both types [8]. Studies have shown that the control of the edge structure of graphene derivatives is critical for tuning GQDs' properties [129,134]. For example, precise control of zigzag edges in graphene nanoribbons (ZGNRs) was accomplished by Ruffieux and collaborators [135,136]. In brief, they employed a polymeric monomer containing bromine halogen functions as a precursor that allowed the formation of a pure zigzag edge structure through an ary-aryl thermally induced reaction. These findings suggested that the edge morphology obtained represented an interesting strategy for tailoring the band structure of devices using GNRs [136]. Tamura et al. tailored the zigzag-edge amount in graphene through exfoliation in supercritical water (SPW) in the presence of Au nanoparticles [137]. The exfoliation by SPW led to the enrichment of zigzag edges and increased the capacitance of graphene. Despite being different materials, the type of edges may also affect GQDs electrochemical sensing performance.

Theoretical investigations of the electronic density of states (DOS) distributions in armchair and zigzag GQDs corroborate the above experimental discoveries for graphene-based compounds. For instance, Zhang and Chang used pure armchair GQDs (AGQDs) and pure zigzag GQDs (ZGQDs) theoretical structures to evaluate the highest valence level (HVL) and the lowest conduction level (LCL) of GQDs [134]. In the DOS graphs of the ZGQDs, an edge state appeared with a size increase, while for AGQDs, this edge state was not present. The authors suggested that the absorption bands can also be modified by turning the edge type, and not only by shape or external magnetic field.

### 5.2. Effect of the Size of GQDs in Their Electrochemical Performance

Optical [138], electrical [139], and biological [140,141] properties of GQDs are intrinsically dependent on their size. For instance, Deng and coauthors demonstrated the influence of size over the electrocatalytic activity of graphene exfoliated via ball milling. The electrocatalytic activity was especially enhanced due to the increment of the specific surface area. However, below 100 nm this enhancement is more evident due to the quantum confinement and edge effect [142].

To evaluate the impact of GQDs' lateral size on optoelectronic properties, Wu et al. synthesized three GQDs with distinct sizes by photon-Fenton reaction, namely GQDs-blue (5.6 nm), GQDs-green (11.2 nm), and GQDs-orange (17.6 nm) [133]. The labels were related to the color of the PL emission of each GQDs sample. In addition, the authors investigated the photovoltaic performance of inverted solar cells based on films of poly(3-hexylthiophene) (P3HT) and poly(3-hexylthiophene)/(6,6)-phenyl-C61butyric acid methyl ester (PCBM) containing GQDs. The short-circuit current density ( $j_{sc}$ ) of the active layer made only of P3HT:PCBM was found to be  $9.57 \text{ mA cm}^{-2}$ , and increased after the addition of GQDs to  $10.33 \text{ mA cm}^{-2}$  (GQDs-blue),  $13.34 \text{ mA cm}^{-2}$  (GQDs-green), and  $11.19 \text{ mA cm}^{-2}$  (GQDs-orange). These changes in the  $j_{sc}$  values confirmed that the lateral size influenced the bandgap of the GQDs. Accordingly, the bandgap values of the GQDs

obtained were 2.72, 2.00, and 1.65 eV for QGDs-blue, QGDs-green, and QGDs-orange, respectively.

Liu et al. evaluated the importance of the size of QGDs on their electrochemical behavior by producing QGDs with sizes of 4.8 nm (QGDs-1), 13.1 nm (QGDs-2), and 34.7 nm (QGDs-3). The different sizes were obtained by changing the ammonia volume used in the hydrothermal synthesis (Figure 4A) [143]. The results revealed a decrease in the PL intensity with size increment using the same excitation wavelength (440 nm). A rectangular shape was obtained in the cyclic voltammograms for the electrode modified with QGDs-1, indicating that the sample with the smaller QGDs exhibited a short diffusion time and consequently an ideal capacitive behavior. Finally, the specific capacitance increased with a particle-sized increment from approximately 5 Faraday per gram ( $F g^{-1}$ ) for QGDs-1 to 88  $F g^{-1}$  for QGDs-3, as shown in Figure 4B.

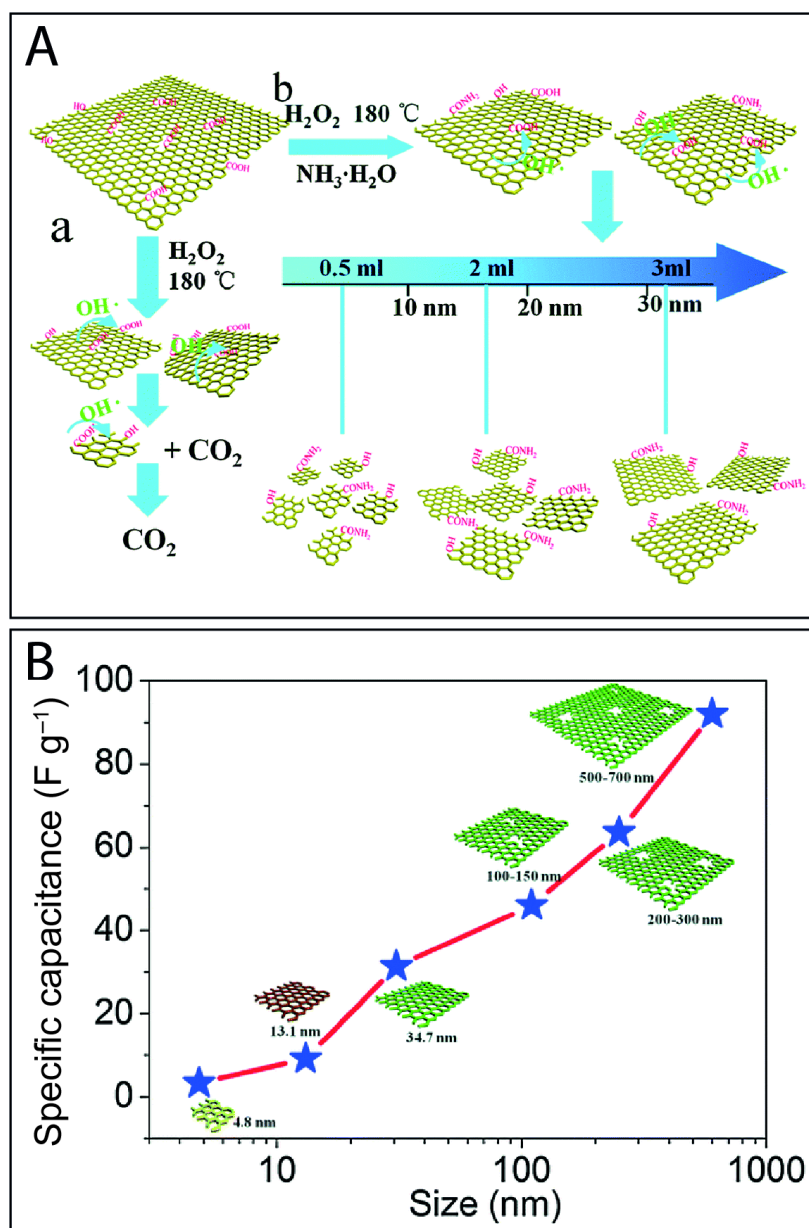


**Figure 4.** (A) Schematic representation of the process to produce QGDs with different sizes and (B) specific capacitance as a function of QGDs size. Reproduced with permission from reference [143]. Copyright 2015 The Royal Society of Chemistry.

Theoretical simulations [144] confirmed that GQD structures terminated with hydrogen in a zigzag edge type with different molecular formulas ( $C_6H_6$ ,  $C_{16}H_{10}$ , and  $C_{24}H_{12}$ ), and consequently distinct sizes, possess different bandgap values, ranging from 4.98 Å to 9.57 Å. Additionally, the authors demonstrated that g- $C_3N_4$ /GQDs composites can be prepared to maximize the photocatalytic performance by tuning the bandgap with different GQDs sizes [144].

In practice, the precise role of the synthesis parameters and the mass production of GQDs with controlled size and edges remain a challenge. In this sense, smaller quantum dots will naturally have a more pronounced edge effect, since they have minor basal planes. Furthermore, the preference for GQDs with an enhanced edge effect or larger basal planes can be tailored depending on the methodology of functionalization employed. Some groups have a preference for tailoring the core, while others for the edge sites [145–147]. As a consequence, elucidating the complete effect of core size and the edges of the GQDs in electrochemical applications has not yet been fully achieved, although some important contributions have been provided in the literature [118,148,149].

## 6. GQDs-Based Nanocomposites Applied in Electrochemical Sensors

In recent years, composites using several functional materials have been developed to improve the electrochemical properties of GQDs [26,150,151]. Considerable enhancement of the sensing performance can be achieved by the combination of GQDs with 0D [73,152–154], 1D [155,156], 2D nanomaterials [96,157], metal–organic frameworks (MOFs) [158,159], molecularly imprinted polymers (MIPs) [160,161], ionic liquids [162,163], and other types of materials, representing a very attractive and favorable strategy for the design of electrochemical interfaces. To date, various GQDs-based nanocomposites have been successfully prepared following different approaches for detecting analytes from ions and small molecules to biomolecules and proteins. The different strategies employed in the development of these materials have been subdivided in this section, while Table 1 summarizes some of the GQDs-based nanocomposite electrochemical (bio)sensors reported in the literature in the past few years.

**Table 1.** Some examples of GQD-based nanocomposites for electrochemical (bio)sensing.

| Electrode Material                      | GQD Preparation Method                          | Target Analyte      | Electrochemical Technique | Linear Range   | LOD                       | Ref.  |
|---|---|---------------------|---------------------------|--|---------------------------|-------|
| Combination with 0D nanomaterials       |   |                     |                           |  |                           |       |
| GQDs/GNPs                               | pyrolysis of CA                                 | luteolin            | DPV                       | 0.01–10 $\mu$ M  | 1.0 nM                    | [164] |
| NH <sub>2</sub> -GQDs/Au- $\beta$ -CD   | commercial source                               | quercetin           | DPV                       | 1–210 nM   | 285 pM                    | [165] |
| NiO/GQD                                 | -   | thioridazine        | DPV                       | 2–200 nM   | 0.05 nM                   | [166] |
| anti-cTnI/AuNPs@GQDs                    | -   | cardiac troponin I  | SWV                       | 5–50 $\text{pg mL}^{-1}$                                 | 0.5 $\text{pg mL}^{-1}$   | [167] |
| AuNPs/N,S-GQDs/aptamer                  | pyrolysis of CA                                 | bisphenol A         | DPV                       | 0.1–10 $\mu$ M   | 0.03 $\mu$ M              | [168] |
| TC-GQD                                  | hydrothermal method from espresso coffee wastes | dopamine            | DPV                       | 0.3–750 $\mu$ M  | 22 nM                     | [169] |
| GQDs@La <sup>3+</sup> @ZrO <sub>2</sub> | pyrolysis of CA                                 | flutamide           | SWV                       | 0.00175–15.75 $\mu$ M                                    | 0.82 nM                   | [170] |
| AgNPs/GQDs                              | ultrasonic method from carbon fibers            | guanine and adenine | DPV                       | guanine: 0.015–430 $\mu$ M<br>adenine: 0.015–390 $\mu$ M | 10 nM 12 nM               | [86]  |
| GQD/AuNP                                | ultrasonic method from carbon black             | quercetin           | DPV                       | 0.01–6.0 $\mu$ M   | 2 nM                      | [79]  |
| Electrode Material                      | GQD Preparation Method                          | Target Analyte      | Electrochemical Technique | Linear Range   | LOD                       | Ref.  |
| anti-AFB1/GQDs-AuNPs                    | pyrolysis of CA                                 | aflatoxin B1        | CV                        | 0.1–30 $\text{ng mL}^{-1}$                               | 0.008 $\text{ng mL}^{-1}$ | [171] |
| Combination with 1D nanomaterials       |   |                     |                           |  |                           |       |

Table 1. Cont.

|  |                                  |  |             |  |  |       |
|--|----------------------------------|--|-------------|--|--|-------|
| GQDs-MWCNTs  | hydrothermal method from GO      | dopamine   | DPV         | 0.005–100 $\mu\text{M}$  | 0.87 nM  | [156] |
| GQDs@MWCNTs  | hydrothermal method from glucose | dopamine   | DPV         | 0.25–250 $\mu\text{M}$   | 95 nM  | [155] |
| PVA/GQD/GOx NFs  | hydrothermal method from GO      | glucose  | amperometry | 0.25–24 mM   | 10 $\mu\text{M}$   | [89]  |
| NGQDs@NCNFs  | pyrolysis of CA                  | nitrite  | DPV         | 5–300 $\mu\text{M}$ and 400–3000 $\mu\text{M}$                                   | 3 $\mu\text{M}$  | [172] |
| NH <sub>2</sub> -GQDs/NiCo <sub>2</sub> O <sub>4</sub> | hydrothermal method from pyrene  | glucose  | amperometry | 1–159 $\mu\text{M}$ and 159–949 $\mu\text{M}$                                    | 0.27 $\mu\text{M}$   | [173] |
| Combination with 2D nanomaterials                      |                                  |  |             |  |  |       |
| GQDs/CoNiAl-LDH  | pyrolysis of CA                  | glucose  | amperometry | 0.01–14.0 mM   | 6 $\mu\text{M}$  | [157] |
| NS-GQD/G   | hydrothermal method from rGO     | H <sub>2</sub> O <sub>2</sub>                        | amperometry | 0.4 $\mu\text{M}$ –33 mM   | 26 nM  | [96]  |
| NH <sub>2</sub> -GQD-GO                                | hydrothermal method from GO      | oxalic acid  | amperometry | 0.5–2.0 mM and 2.0–55 mM   | 50 $\mu\text{M}$   | [174] |
| Combination with other types of materials              |                                  |  |             |  |  |       |
| ds-DNA-IL/GQDs   | pyrolysis of CA                  | topotecan  | DPV         | 0.35–100 $\mu\text{M}$   | 0.1 $\mu\text{M}$  | [87]  |
| RTIL-GQDs  | pyrolysis of CA                  | levodopa   | SWV         | 0.05–250 $\mu\text{M}$   | 10 nM  | [162] |
| GQDs/IL  | pyrolysis of CA                  | ascorbic acid (AA), dopamine (DA) and uric acid (UA) | DPV         | AA: 25–400 $\mu\text{M}$<br>DA: 0.2–10 $\mu\text{M}$<br>UA: 0.5–20 $\mu\text{M}$ | AA: 6.64 $\mu\text{M}$<br>DA: 0.06 $\mu\text{M}$<br>UA: 0.03 $\mu\text{M}$ | [163] |
| MIPPy/GQDs   | hydrothermal method from GO      | bisphenol A  | DPV         | 0.1–50 $\mu\text{M}$   | 0.04 $\mu\text{M}$   | [175] |
| m-GQDs-MIP   | hydrothermal method from GO      | ifosfamide   | DPASV       | 0.25–121.35 ng mL <sup>-1</sup>  | 0.08 ng mL <sup>-1</sup>   | [160] |
| GQD-PCN-222  | electrochemical method           | nitrite  | amperometry | 40–18.000 $\mu\text{M}$  | 6.4 $\mu\text{M}$  | [158] |
| $\beta$ -CD@N-GQD                                      | hydrothermal method from CA      | cholesterol  | DPV         | 0.5–100 $\mu\text{M}$  | 80 nM  | [176] |
| Combination with more than one type of materials       |                                  |  |             |  |  |       |
| GQDs-PSSA/GO   | pyrolysis of CA                  | estradiol (E2) and progesterone (P4)                 | DPV         | E2: 0.001–6.0 $\mu\text{M}$<br>P4: 0.001–6.0 $\mu\text{M}$                       | 0.23 nM<br>0.31 nM   | [177] |
| Fe <sub>3</sub> O <sub>4</sub> @GQD/f-MWCNTs           | pyrolysis of CA                  | progesterone   | DPV         | 0.01–0.5 and 0.5–3.0 $\mu\text{M}$   | 2.18 nM  | [178] |
| AuNPs/GQDs-WS <sub>2</sub>                             | commercial source                | malachite green                                      | DPV         | 0.01–10 $\mu\text{M}$  | 3.38 nM  | [179] |
| hNiNS/GQDs/MIPs  | hydrothermal method from rGO     | bisphenol S  | DPV         | 0.1–50 $\mu\text{M}$   | 0.03 $\mu\text{M}$   | [180] |
| Au NSs/GQDs-CS/cysteamine                              | pyrolysis of CA                  | ractopamine  | DPV         | 0.0044 fM–19.55 $\mu\text{M}$  | 0.0044 fM  | [181] |
| MIP-AuNPs/N,S@GQDs                                     | pyrolysis of glucose             | sofosbuvir   | DPV         | 1–400 nM   | 0.36 nM  | [161] |
| (mag@MIP)-GQDs-FG-NF                                   | pyrolysis of CA                  | ethinylestradiol                                     | SWV         | 10 nM–2.5 $\mu\text{M}$  | 2.6 nM   | [182] |
| MoS <sub>2</sub> @N-GQDs-IL MIP                        | pyrolysis of CA                  | IgG  | DPV         | 0.1–50 ng mL <sup>-1</sup>   | 0.02 ng mL <sup>-1</sup>   | [183] |
| NMO/GQDs/CS  | pyrolysis of CA                  | diazinon   | DPV         | 0.1–330 $\mu\text{M}$  | 27 nM  | [184] |
| LaNPs-GQDs@ZIF-8                                       | pyrolysis of CA                  | vitamin D <sub>3</sub>                               | SWV         | 0.00625 $\mu\text{M}$ –1.25 $\mu\text{M}$  | 6.1 nM   | [185] |
| PPy/GQDs@PB  | pyrolysis of CA                  | L-cysteine   | amperometry | 0.2–50 $\mu\text{M}$ and 50–1000 $\mu\text{M}$                                   | 0.15 $\mu\text{M}$   | [186] |

Table 1. Cont.

| Electrode Material       | GQD Preparation Method                           | Target Analyte                | Electrochemical Technique | Linear Range   | LOD                              | Ref.  |
|--------------------------|--|-------------------------------|---------------------------|--|----------------------------------|-------|
| MIP/Au@Cu-MOF/N-GQDs     | pyrolysis of CA                                  | patulin                       | DPV                       | 0.001–70.0 ng mL <sup>-1</sup>                               | 0.0007 ng mL <sup>-1</sup>       | [159] |
| PS-PNIPAm-PS/MWCNTs-GQDs | comercial source                                 | paracetamol                   | DPV                       | 0.1–7.0 μM and 7.0–103 μM                                    | 66 nM                            | [187] |
| GQD-PNF-GO               | electrolysis of graphite rod                     | H <sub>2</sub> O <sub>2</sub> | amperometry               | 0.01–7.2 mM  | 0.055 μM                         | [188] |
| N,S-GQDs@AuNP-PAni       | hydrothermal method with thiourea to citric acid | hepatitis E virus             | impedance                 | 10 <sup>2</sup> –10 <sup>7</sup> RNA copies mL <sup>-1</sup> | 96.7 RNA copies mL <sup>-1</sup> | [189] |

LOD—limit of detection; NPs—nanoparticles; CA—citric acid; SWV—square wave voltammetry; GNPs—gold nanoparticles; DPV—differential pulse voltammetry; Au-β-CD—thiolated β-cyclodextrin functionalized gold nanoparticles; anti-cTnI—cardiac troponin-I antibody; TC—titania-ceria; anti-AFB1—antibody of aflatoxin B1; MWCNT—multiwalled carbon nanotubes; GOx—glucose oxidase; NFs—nanofibers; NCNFs—N-doped carbon nanofibers; LDH—layered double-hydroxide; G—graphene; ds-DNA—double stranded DNA; IL—ionic liquid; LSV—linear-sweep voltammetry; RTIL—room temperature ionic liquid; MIPPy—molecularly imprinted polypyrrole; DPASV—differential pulse anodic stripping voltammetry; PCN-222—mesoporous porphyrinic zirconium-based metal–organic framework; β-CD—β-cyclodextrin; MIP—molecularly imprinted polymer; PSSA—poly(sulfosalicylic acid); GO—graphene oxide; f-MWCNTs—functionalized multi-walled carbon nanotubes; hNiNS—hollow nickel nanospheres; NSs—nanostructures; CS—chitosan; mag@MIP—magnetic nanoparticles coated with molecularly imprinted polymers; FG—functionalized graphene; NF—Nafion®; NMO—nickel molybdate nanocomposites; LaNPs—lanthanum nanoparticles; ZIF-8—zeolitic imidazolate frameworks; PPy—polypyrrole; PB—prussian blue; Au@Cu-MOF—AuNPs-functionalized Cu-metal organic framework; PS-PNIPAm-PS—thermosensitive polymer poly(styrene-*b*-(N-isopropylacrylamide)-*b*-styrene); PNF—peptide nanofibers; AuNP-PAni—gold-embedded polyaniline nanowires.

### 6.1. GQDs Combined with 0D Nanomaterials

The use of 0D nanostructures as electroactive materials for the construction of electrochemical devices is of great interest in view of their unique electronic and surface properties. Because of such characteristics, an increasing number of studies on 0D nanomaterials applied in (bio)sensors has been reported in the past few years [190]. In this scenario, several authors have demonstrated that hybridizing metal oxide, e.g., Fe<sub>3</sub>O<sub>4</sub> [73,152], Co<sub>3</sub>O<sub>4</sub> [191], NiO [77,166], ZnO [192], ZrO<sub>2</sub> [170], and metal nanoparticles (NPs), such as Au [153,154], Ag [193–195], and AuPd [78] with GQDs can enhance their sensing performance in terms of sensitivity and selectivity. Among these nanomaterials, Au NPs and Ag NPs are the most employed, due to their excellent conductivity, high surface area, biocompatibility, and catalytic activity [79,196]. In this regard, an electrochemical sensor based on GQDs and gold nanoparticles (GNPs) was developed for the determination of luteolin, a polyphenolic compound available in foods of plant origin with antioxidant, anti-inflammatory, and antibacterial activities [164]. The modified glassy carbon electrode (GCE) was prepared in two steps: First, the GNPs were electrochemically deposited on the bare GCE, and then GQDs were electrodeposited onto the GNPs' modified electrode. As illustrated in Figure 5A(i), CV studies revealed that the redox peak currents of luteolin obtained with the electrode modified with the hybrid material (GQDs/GNPs/GCE) were increased 16-fold and 1.5-fold compared to that of the bare GCE and GQDs/GCE, respectively, which suggests the excellent synergetic effect of GNPs and GQDs. The improved performance was mainly attributed to three contributing factors: (i) The good conductivity of GNPs, (ii) the high electroactive surface area of GQDs, and (iii) the enrichment effect of the electrode surface for the analyte. In addition, the authors demonstrated that two electrons were involved in the electrochemical redox process of luteolin at the modified electrode (Figure 5A(ii)). The GQDs/GNPs/GCE showed remarkable performance in terms of limit of detection (LOD) and linear range, as illustrated in Table 1. Additionally, the proposed sensor was also demonstrated to be applicable for the detection of the luteolin content in peanut hulls with recovery of 98.8–101.4%.

The combination of GQD with noble metal nanomaterials has also been considered a suitable choice for the detection of analytes of environmental [168,197] and biomedical interest [79,86,154,167,198]. For instance, Shadjou et al. reported the development of an electrochemical sensing platform based on Ag NPs and nitrogen-doped GQDs (N-GQDs) for sensitive voltammetric detection of nicotinamide adenine dinucleotide (NAD) in human plasma samples [198]. The authors showed that the response of NAD was improved when

Ag NPs were introduced to the structure of the N-GQDs-GCE, and an LOD of 0.33 fM was obtained. The improvement may be related to the advantageous properties of N-GQDs, such as high surface area and  $\pi$ - $\pi$  interaction with GCE, which facilitated the electron transfer mechanism, and the electrical conductivity of the Ag NPs.

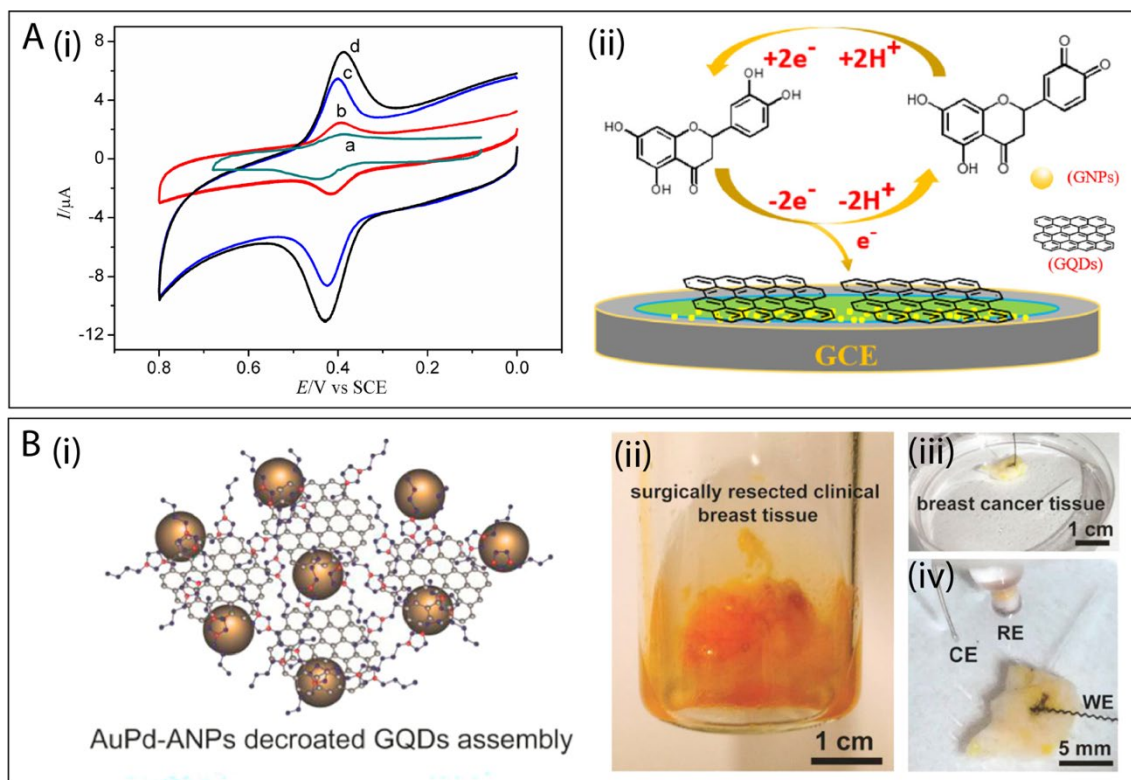


**Figure 5.** (A) (i) Cyclic voltammograms of the (a) bare GCE, (b) GNPs/GCE, (c) GQDs/GCE, and (d) GQDs/GNPs/GCE in 0.1 M phosphate buffer (pH 5.0) containing 20  $\mu\text{M}$  luteolin at scan rate of 100  $\text{mV s}^{-1}$  and (ii) the proposed electrochemical reaction process of luteolin onto GQD/GNPs/GCE surface. Reproduced with permission from reference [164]. Copyright 2019 Elsevier. (B) (i) Schematic illustration of AuPd-ANPs decorated GQDs assembly and digital photographs of (ii) the surgically resected clinical breast specimen from a female patient with primary breast cancer, (iii) the breast cancer tissue, and (iv) the three-electrode setup for tissue measurement, with a AuPd-ANPs/GQDs microelectrode as WE, Ag/AgCl as RE, and Pt wire as CE. The flexible AuPd-ANPs/GQDs microelectrode was wound into a helical shape and inserted in the breast cancer tissue. Reproduced with permission from reference [78]. Copyright 2018 Elsevier.

Benefiting from the unique structural merits of AuPd alloy nanoparticles (AuPd-ANPs) and GQDs assembly through electrodeposition, and the synergistic effect of dual electroactivities towards  $\text{H}_2\text{O}_2$ , Xu and coworkers reported the application AuPd-ANPs/GQDs nanocomposite (Figure 5B(i)) for real-time tracking of  $\text{H}_2\text{O}_2$  secreted from living human breast cancer cells [78]. The modified electrode exhibited a high sensitivity, a linear range from 1.0  $\mu\text{M}$  to 18.44 mM, low LOD of 500 nM, as well as good selectivity and biocompatibility. Furthermore, the practicability of the AuPd-ANPs/GQDs/ACF microelectrode was verified by in situ detection of the cancer biomarker in clinical breast cancer tissue (Figure 5B(ii)). For the detection of  $\text{H}_2\text{O}_2$  secreted from living cancer cells in breast cancer tissue, the microelectrode was wound into a helical shape and inserted inside the breast cancer tissue, as shown in Figure 5B(iii–iv).

Metal oxide nanoparticles have also been applied in GQDs-based sensors due to their high surface-to-volume ratio, high surface reaction activity, high catalytic efficiency, strong adsorption ability, and electron and phonon confinements [199,200]. In this direction, Shamsi et al. reported the synthesis of a NiO/GQD nanocomposite by electrodeposition and its application as an ultrasensitive electrochemical platform for the detection of

clozapine, an antipsychotic drug [77]. Their study revealed that the oxidation current of clozapine at the surface of a NiO/GQD composite-modified electrode increased compared to that of the bare GCE and GQD-modified GCE. This improvement in the electrochemical performance was attributed to the fast heterogeneous electron transfer kinetics, larger accessible surface, and numerous active sites at the surface of the nanocomposite, arising from the synergic coupling between the excellent catalytic effect of NiO nanoparticles and high density of edge sites of GQDs. Voltammetry studies showed that the anodic peak current increased linearly with clozapine concentration in the range of 3 to 1000 nM, and the LOD was found to be 0.55 nM.

### 6.2. GQDs Combined with 1D Nanomaterials

1D nanomaterials such as nanowires, nanotubes, nanoribbons, nanorods, and nanofibers have emerged as an exciting class of nanomaterials for constructing efficient electrochemical devices [201]. Recently, studies have shown that the charge transfer between the 1D nanomaterials and analyte molecules can be improved by their surface-functionalization with GQDs [155,156]. For example, Huang et al. reported an electrochemical sensor with high sensitivity and selectivity for measuring dopamine (DA) using GQDs-multiwalled carbon nanotubes (GQDs/MWCNTs) composite-modified GCE [156]. As depicted in Figure 6A(i), the redox peak currents at the GQDs-MWCNTs/GCE increased compared to GCE and MWCNTs/GCE. The authors attributed this improved performance to (i) the presence of anionic groups in the GQDs (oxygen functionalities), which are beneficial for enhancing sensitivity for the determination of DA by electrostatic attractions with cations and (ii) the presence of cation- $\pi$  interaction between conjugated  $\pi$  bonds in the GQDs-MWCNTs and the oxidized state of DA. As shown in Figure 6A(ii), the nanocomposite was able to detect DA secreted from live PC12 cells. The effect of MWCNTs on the electrochemical sensing performance of GQDs was also investigated by Arumugasamy and coworkers [155]. The introduction of MWCNTs not only improved the electrochemical signal of DA, but also increased the GQDs catalytic activity. The dual signal enhancement facilitated the construction of a ratiometric electrochemical sensor for the detection of DA. In addition, the developed electrochemical sensor displayed high selectivity towards common interferences, like glucose, glutamic acid, KCl, and ascorbic acid, and was able to detect DA in human serum samples.

In another work, NiCo<sub>2</sub>O<sub>4</sub>/GQDs nanoneedles were successfully applied for nonenzymatic glucose detection [173]. The addition of GQDs greatly enhanced the electrocatalytic performance of NiCo<sub>2</sub>O<sub>4</sub> due to the higher electron transfer ability of the nanocomposite. The synergy between the two materials led to a nanocomposite-based electrode with remarkable sensitivity of 1185.58  $\mu\text{A mm}^{-1} \text{cm}^{-2}$  in the linear concentration range from 1 to 159  $\mu\text{M}$  and 2521.33  $\mu\text{A mm}^{-1} \text{cm}^{-2}$  in the linear range of 0.159–0.949  $\mu\text{M}$  toward the glucose oxidation, respectively. In addition, the NiCo<sub>2</sub>O<sub>4</sub>/GQDs/CC electrode also presented a low LOD of 0.27  $\mu\text{M}$  for glucose detection.

GQDs-based nanocomposites have also been applied as ECL probes [26,202]. Through the combination of GQDs with titanium dioxide nanotubes (TiO<sub>2</sub> NTs), Tian et al. developed an ECL sensor for the sensitive and selective determination of prostate protein antigen (PSA) [203]. When compared to the pristine TiO<sub>2</sub> NTs, the nanocomposite exhibited a 6-fold enhancement of ECL intensity and a decrease by 300 mV of the ECL onset potential, which are ascribed to the GQDs presence. The authors observed that the ECL intensity decreased with the increase of PSA concentration in the range from 1.0  $\text{fg mL}^{-1}$  to 10  $\text{pg mL}^{-1}$ , with a lower LOD of 1  $\text{fg mL}^{-1}$ . Furthermore, PSA could be detected in clinical serum samples of prostate cancer patients and controls with excellent correlation to the reference chemiluminescence method.

The incorporation of GQDs into electrospun nanofibers has also been used as an efficient strategy to design electrochemical sensors [8,82]. In this context, an all-carbon-based composite consisting of N-doped GQDs decorated on the N-doped carbon nanofibers (NGQDs@NCNFs) surface was prepared by electrospinning, post-annealing, and the hy-

drothermal method, and applied in an electrochemical sensor for nitrite determination [172]. The NCNFs acted as support for NGQDs attachment, avoiding the large aggregation of NGQDs and hence maintaining their large electroactive surface area and abundant active sites. Moreover, electrochemical studies showed that upon introducing NCNFs, the conductivity of NGQDs@NCNFs composite was sharply improved in comparison with NGQDs alone or the mixture of NGQDs and NCNFs, leading to a fast electron transfer rate between the modified electrode and the electrolyte. The developed electrochemical sensor displayed a wide linear range and a low LOD towards nitrite in sausage, pickle, lake water, and tap water, suggesting its suitability for food and environmental analyses. In the same fashion, GQDs were incorporated into polyvinyl alcohol (PVA) nanofibers aiming at electrochemical detection of  $\text{H}_2\text{O}_2$  [89]. The GQD/PVA fibers were directly electrospun onto the GCE. The wide linear range and the low LOD obtained were ascribed to the presence of GQDs, whose functional groups acted as stable catalysts during the redox reactions.

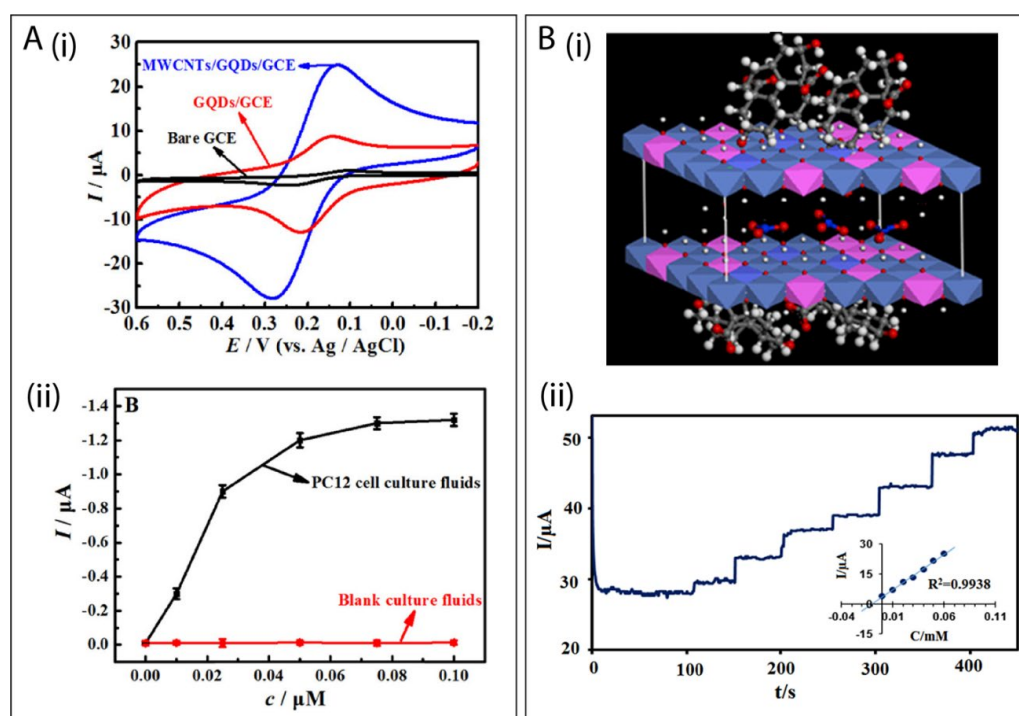


**Figure 6.** (A) (i) Cyclic voltammograms of GCE, GQDs/GCE, and MWCNTs/GQDs/GCE in 0.1 mM DA (scan rate of  $0.1 \text{ V s}^{-1}$ ) and (ii) the anodic peak current ( $I_{\text{pa}}$ ) of DA in the PC12 cells cultures. Reproduced with permission from reference [156]. Copyright 2020 American Chemical Society. (B) (i) Proposed structure of GQDs/CoNiAl-LDH nanocomposite and (ii) amperometric responses of the GQDs/CoNiAl-LDH/CPE towards mango juice samples upon successive additions of 0.02 mM of glucose standard solution in 0.1 M NaOH at an applied potential of 0.1 V. Insets show the linear dependence of currents as a function of glucose concentrations. Reproduced with permission from reference [157]. Copyright 2017 Elsevier.

### 6.3. GQDs Combined with 2D Nanomaterials

2D nanomaterials display unique chemical/physical properties, including large surface area, high chemical stability, easy functionalization, high electrical conductivity, and mechanical strength due to their graphene-like structures [204,205], which makes them materials with good potential to be used in sensing applications. Furthermore, functional groups on the surface of these materials offer versatile approaches to couple chemical/biological molecular receptors for biosensing assays [205]. Moreover, recent studies have shown that other materials can be used as effective building blocks in the preparation of multifunctional composites to further boost the electrical conductivity and electrocat-

alytic performance of 2D nanomaterials [206]. In this sense, a composite of GQD co-doped with N and S atoms (NS-GQD) and graphene was synthesized and applied as a sensing probe for  $\text{H}_2\text{O}_2$  [96]. The GQDs were firstly self-assembled on graphene nanoplatelets (G) via hydrothermal treatment, and then a thermal annealing procedure using the hybrid nanosheets and thiourea was employed to form the NS-GQD/G hybrid nanosheets. The authors found that when GQDs were uniformly distributed on graphene sheets, they served as highly conductive substrates to interconnect the GQDs for efficient electron transfer. In addition, the abundant oxygen-containing functional groups and the exposed edges of GQDs provided more active sites for  $\text{H}_2\text{O}_2$  electrocatalytic reduction. More importantly, microscope images revealed that the flakelike structure of the NS-GQD/G nanocomposite with a crinkled and curved surface was loosely packed, which permitted accessible transport of supporting electrolyte and electro-reactants/products, and enhanced the electrochemical performance of NS-GQD/G. These factors endow NS-GQD/G with ultrahigh performance towards  $\text{H}_2\text{O}_2$  electrocatalysis reduction. Besides the linear range and the low LOD obtained, practical application of the NS-GQD/G sensor was effectively assessed for the detection of  $\text{H}_2\text{O}_2$  in human serum samples and that released from Raw 264.7 cells.

Some layered compounds, such as layered double-hydroxides (LDHs), can suffer from low conductivity, which restricts electron transfer and hinders their electrocatalytic performance [207,208]. To solve this problem, Samuei et al. reported the use of GQDs as 0D building block to enhance the electron transport rate, electrolyte contact area, conductivity, and structural stability of CoNiAl-layered double-hydroxide [157]. In their work, a nanocomposite based on the GQDs and CoNiAl-LDH (GQDs/CoNiAl-LDHs) (Figure 6B(i)) was successfully synthesized by the co-precipitation method. The GQDs/CoNiAl-LDH exhibited a significant synergistic electrocatalytic activity compared to CoNiAl-LDH. The strong association of the CoNiAl-LDH with GQDs facilitated charge transport and improved the electrocatalytic activity towards glucose oxidation. At optimal conditions, the constructed sensor exhibited a wide linear range (0.01–14 mM) with an LOD of 6 mM and high sensitivity of  $48.717 \text{ mA mM}^{-1}$ . Moreover, as depicted in Figure 6B(ii), the GQDs/CoNiAl-LDH-modified carbon paste electrode was able to detect trace amounts of glucose in juice samples.

Du and coworkers explored the use of GQDs-based nanocomposite for environmental sensing [209]. In their report, GO decorated with NGQDs (NGQDs-GO) was prepared by combining thermal and hydrothermal treatments for the ECL detection of pentachlorophenol (PCP). The NGQDs-GO nanocomposite showed more outstanding ECL performances than the pristine counterparts. Moreover, the interaction between PCP and the nanocomposite resulted in a remarkable change in the ECL intensity, allowing the detection of PCP in a wide linear range from 0.1 to  $10 \text{ pg mL}^{-1}$  with a low LOD of  $0.03 \text{ pg mL}^{-1}$ . The practicability of the sensing platform was also evaluated towards real water samples.

It is important to mention that, despite the great potential of 2D nanomaterials to improve the sensitivity and performance by facilitating the electron transfer process and signal generation, until now, very few works reported electroanalytical investigation of electrodes modified with GQDs combined with 2D nanomaterials, which is, therefore, a research area to be explored.

#### 6.4. GQDs Combined with Other Types of Materials

GQDs have also been combined with 3D nanostructures [158,210], ionic liquids [87,162,163], MIPs [160,175], and other materials to exploit the nanocomposite material features in electrochemical applications, as illustrated in this section.

Ionic liquids (ILs) are defined as materials composed of cations and anions that melt around  $100 \text{ }^\circ\text{C}$  or below an arbitrary temperature limit. A typical IL has a bulky organic cation that is weakly coordinated by an organic or inorganic anion [211]. Properties such as high conductivity, good catalytic activity, long-term electrochemical and thermal stability of ILs make them ideal for electrochemical sensors [211,212]. Additionally, ILs are good dispersants of carbon nanomaterials, including GQDs, which help the formation of a

uniform electrode structure with well-distributed components, consequently leading to a significant improvement in electrochemical performance. [213]. In this direction, Kuntee et al. combined GQDs and IL for the simultaneous electrochemical determination of ascorbic acid (AA), dopamine (DA), and uric acid (UA) [163]. As shown in Figure 7A, when IL and GQDs were separately used to modify screen-printed carbon electrodes (SPCE), the responses obtained were not good enough for measuring these three species. When both GQDs and IL were used to modify the SPCE surface, well-defined and distinguishable sharp peaks of three electroactive species appeared at  $-0.02$ ,  $0.18$ , and  $0.36$  V, respectively. Furthermore, the oxidation peak currents were remarkably increased when using the GQDs/IL-SPCE. The results indicated that the GQDs/IL-SPCE combined the electrochemical properties of IL and GQDs, allowing the simultaneous determination of the three analytes, as demonstrated in Table 1.

Cyclodextrins (CDs) are oligosaccharides consisting of six, seven, or eight glucose units (named  $\alpha$ -,  $\beta$ -, or  $\gamma$ -CD, respectively), which present a toroidal form with a hydrophobic inner cavity and a hydrophilic exterior [214]. They are promising candidates to be used as functional units in the fabrication of electrodes for electrochemical applications due to their supramolecular recognition [215,216]. Therefore, nanocomposites obtained from the combination of GQDs and CDs are expected to present advantageous “mixed” properties, including large surface area, high electrical conductivity, and enhanced supramolecular recognition capability. With this in mind, different authors have explored the structures and complementary properties of CDs and GQDs to develop different electrochemical sensors to detect distinct analytes, including tyrosine enantiomers [217], nitroaniline isomers [218] vitamin C at physiological pH [217], cholesterol [176], and aflatoxin M1 in milk samples [219].

MOFs are 3D nanomaterials that have attracted great attention due to their unique characteristics, such as regular and interconnected porosity, ultrahigh specific surface area, and intraframework chemical functionality [220]. However, the electrically insulating nature of most MOFs might hamper their practical use in electrochemical and electronic applications. To overcome this limitation, GQDs with an average size of 3.1 nm were incorporated into a mesoporous porphyrinic mesoporous zirconium-based MOF, PCN-222, by employing an impregnation method (Figure 7B(i)) [158]. The GQD-PCN-222 hybrid material showed a 100-fold higher electrical conductivity compared to that of the pristine MOF and exhibited a much better activity for electrochemical sensing towards nitrite compared to that of both the pristine GQD and MOF, as illustrated in Figure 7B(ii). The fabricated platform was suitable for monitoring nitrite by amperometry (Figure 7B(iii)) in a wide linear range with an LOD of  $6.4 \mu\text{M}$ . In another work, GQDs were synthesized on the surface of  $\text{Cu}_2\text{O}$ -CuO hexapod-like (3D) structure via self-assembly, as illustrated in Figure 7C [210]. Benefitting from the synergistic effects of the enhanced active surface area, high conductivity, more exposed {111} facets of hexapod structure, and fast redox reaction due to  $\pi$ -electron delocalization of GQDs, the heterostructures offered outstanding electrocatalytic abilities compared to the pristine materials. The electrochemical sensor displayed a low LOD ( $\leq 1$  nM), good chemical stability over a broad linear range ( $2$  nM– $11$  mM), allowing the BPA detection in water and human serum samples.

The combination of GQDs with MIPs is also an interesting strategy for the development of electrochemical (bio)sensors. MIPs are synthetic polymers typically obtained by copolymerization of a monomer with a cross-linker in the presence of a template molecule. MIPs have been used as an artificial recognition material whose binding site size and shape are complementary to the template molecules for their specific recognition [221]. Different authors have reported that the detection sensitivity of an imprinted sensor can be improved by the use of carbon-based nanomaterials, including GQDs [160,175,222]. In this regard, Prasad et al. reported the synthesis of a nanocomposite based on functionalized GQDs and imprinted polymer at the surface of SPCE using N-acryloyl-4-aminobenzamide as a functional monomer and an anticancer drug (ifosfamide) as a template molecule [160]. Differential pulse anodic stripping voltammetry (DPASV) studies revealed that the anodic

stripping signal was enhanced by a GQDs-based imprinted sensor about 7-fold when compared to the MIPs prepared in the absence of GQDs. This improved performance was attributed to the covalent attachment of GQDs to the monomer molecules, which provides a good pathway for electron transport. The proposed sensor showed improved performance for the analysis of ifosfamide in real (biological/pharmaceutical) samples with a low LOD, without any matrix effect, cross-reactivity, and false positives.

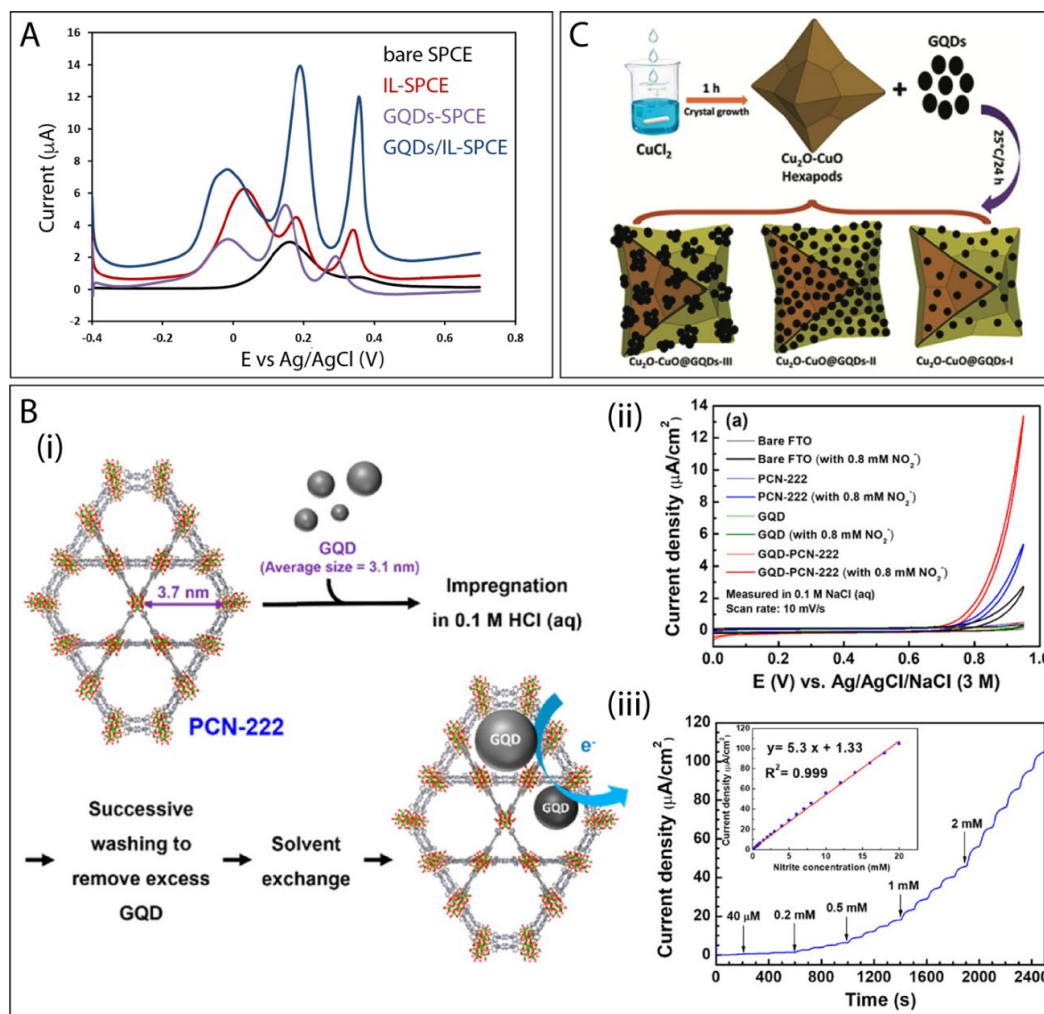


**Figure 7.** (A) DPVs of bare SPCE, IL-SPCE, GQDs-SPCE, and GQDs/IL-SPCE in 0.1 M PBS (pH 4.0) containing 400  $\mu\text{M}$  AA, 10  $\mu\text{M}$  DA, and 10  $\mu\text{M}$  UA. Reproduced with permission from reference [163]. Copyright 2020 Elsevier. (B) (i) Schematic illustration of the incorporation of GQD into PCN-222 via direct impregnation, (ii) CV curves of the PCN-222 thin film, GQD-PCN-222 thin film, GQD thin film, and the bare FTO substrate, measured in 0.1 M NaCl aqueous solutions with or without adding nitrite, and (iii) amperometric curve recorded for the GQD-PCN-222 thin-film during successive droppings of the nitrite in a 0.1 M NaCl aqueous solution. Applied potential: +0.9 V. The inset shows the plot of current density vs. concentration of nitrite along with the calibration curve. Reproduced with permission from reference [158]. Copyright 2019 American Chemical Society. (C) Schematic presentation of the synthesis of core-shell  $\text{Cu}_2\text{O-CuO}@\text{GQD}$  extended hexapod heteroarchitectures prepared via self-assembly. Reproduced with permission from reference [210]. Copyright 2019 The Royal Society of Chemistry.

### 6.5. GQDs Combined with More Than One Type of Material

In recent years, several studies suggested that the combination of more than one type of material might be a superior strategy to boost the electrochemical properties of GQDs. Several combinations have been already reported, as can be seen in Table 1. For instance, Xi et al. reported the incorporation of Pd NPs with an average size of 2.9 nm and nitrogen-

doped GQD (NGQD) into N-doped carbon hollow-structured nanospheres (NC-HNSs) architecture, resulting in a hybrid material (NGQD@NC@Pd HNS), which was applied as a nanoprobe for H<sub>2</sub>O<sub>2</sub> sensing [223]. The hybrid material was synthesized by an efficient five-step synthetic procedure illustrated in Figure 8A(i). Owing to the synergistic effect from the structural and compositional merits of catalytically active species and the HNS supports, the hybrid material showed a large surface area, fast electron transfer rate, and an enhanced electrocatalytic activity towards H<sub>2</sub>O<sub>2</sub> reduction (Figure 8A(ii)). Consequently, the H<sub>2</sub>O<sub>2</sub> sensor based on NGQD@NC@Pd HNSs exhibited a collection of highly desirable sensing performances with a sensitivity of 0.59 mA cm<sup>-2</sup> mM<sup>-1</sup>, an LOD of 20 nM, and selectivity to H<sub>2</sub>O<sub>2</sub> in the presence of common interferents (e.g., dopamine, uric acid, and ascorbic acid). In addition, the proposed biosensing system demonstrated practical ability to distinguish a trace amount of H<sub>2</sub>O<sub>2</sub> released from various living cancer cells. Further aiming at the detection of H<sub>2</sub>O<sub>2</sub>, Li et al. designed a ternary nanocomposite based on GQD, peptide nanofibers, and graphene oxide (GQD-PNF-GO) [188]. The authors attributed the wide linear detection range and the low LOD to the presence of PNFs between graphene layers, which provided a larger surface area for electrolytes adsorption and reactants diffusion and enhanced the performance of the fabricated sensor.

In another work, a nanocomposite based on anti-hepatitis E virus antibody-conjugated to nitrogen- and sulfur-co-doped graphene quantum dots (Ab-N,S-GQDs), gold nanoparticles, and polyaniline nanowires (Ab-N,S-GQDs@AuNP-PAni) were developed and applied for the impedimetric detection of hepatitis E virus (HEV) [189]. The authors demonstrated that the presence of N,S-GQDs improved the electrochemical response and provided enhanced active sites for the target HEV. In addition to the low LOD achieved, the sensor showed extremely good selectivity to HEV in the presence of other viruses, serum, and even culture medium.

Imprinted technology has also been proven to be an ideal method to prepare multicomponent GQD-based nanomaterial for electrochemical applications. In this regard, MIP film based on nitrogen-doped GQDs (N-GQDs), Au NPs, and MOF (Au@Cu-MOF/N-GQDs) was developed and employed for the detection of patulin, a mycotoxin of potential concern found in food [159]. This synergistic effect of N-GQDs and Au@Cu-MOF combined with the MIP technique offered outstanding sensing properties for the detection of patulin in apple juice with good accuracy (recovery of 97.6–99.4%) and high precision (RSD of 1.23–4.61%). Recently, a hybrid material based on MIP-decorated CuFe<sub>2</sub>O<sub>4</sub> nanoparticles for specific detection of human immunoglobulin G (IgG) was reported by Liang and coworkers [183]. In addition, the authors prepared a layered MoS<sub>2</sub>@N-GQDs-IL nanocomposite membrane (Figure 8B) for signal amplification. The GCE modified with the MIP-decorated CuFe<sub>2</sub>O<sub>4</sub> modified with MoS<sub>2</sub>@N-GQDs-IL showed an increased peak current, demonstrating that the composite membrane played a role as a highly effective promoter in enhancing the IgG electrochemical performance. Benefiting from the strong electrostatic chemical interactions between ionic liquid and MoS<sub>2</sub>@N-GQDs and the improvement of dispersion of MoS<sub>2</sub>@N-GQDs by the IL, the nanocomposite provided an effective platform for analyzing IgG content in the human serum specimens. Under optimized experimental conditions, the sensor shortened the response time to less than 8 min, and the response was linear at the IgG concentration of 0.1–50 ng mL<sup>-1</sup> with a LOD of 0.02 ng mL<sup>-1</sup>.

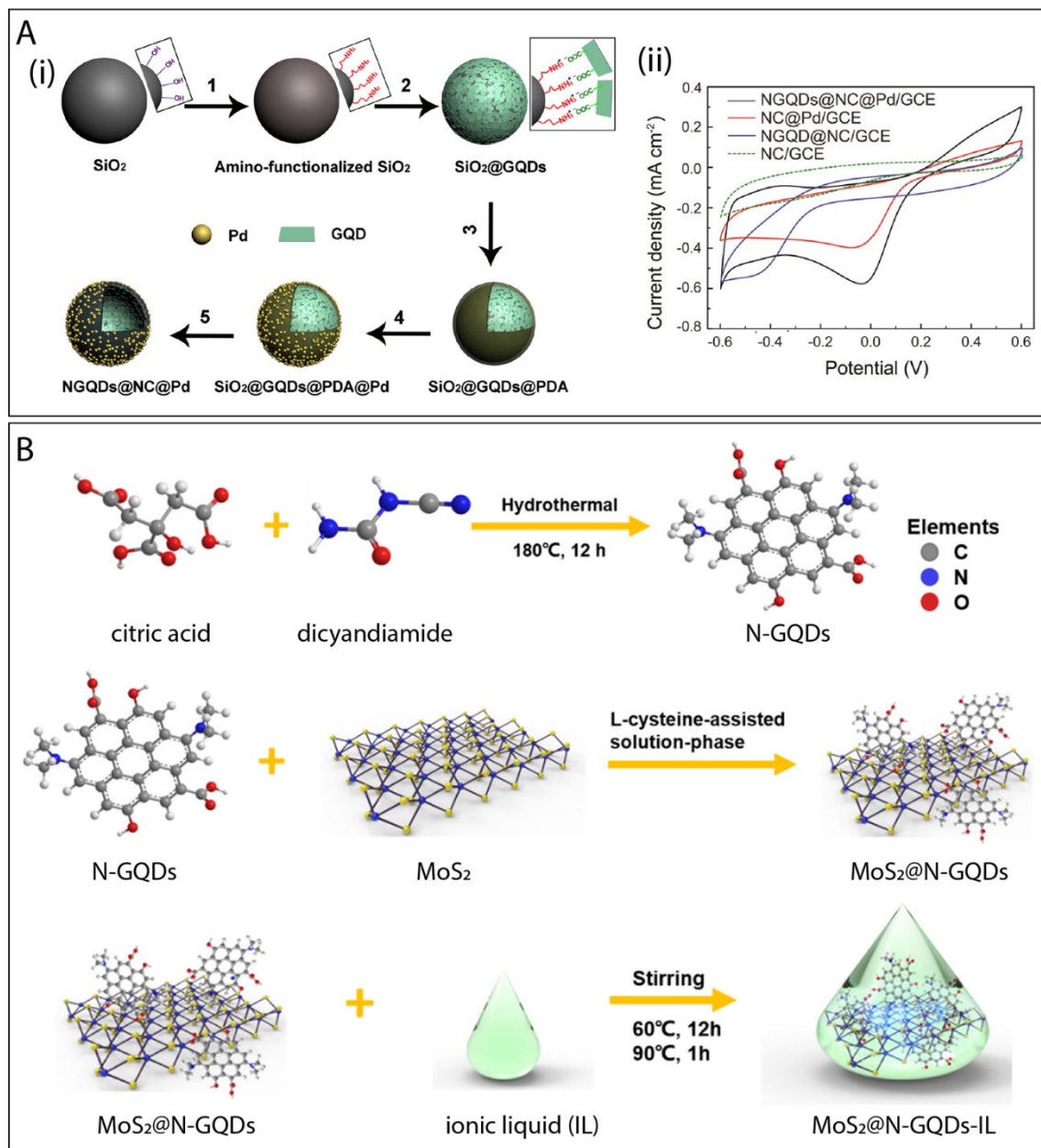


**Figure 8.** (A) (i) Schematics illustrating the preparation process of NGQDs@NC@Pd HNSs: (1) Amino functionalization of SiO<sub>2</sub> nanospheres; (2) wrapping SiO<sub>2</sub> nanospheres with GQD nanosheets; (3) coating of PDA on the surface of SiO<sub>2</sub>@GQD; (4) loading of Pd NPs on the surface of SiO<sub>2</sub>@GQD@PDA; (5) further carbonization and HF etching to form NGQD@NC@Pd HNSs and (ii) CV curves of the nanocomposites in PBS containing 1.0 mmol L<sup>-1</sup> H<sub>2</sub>O<sub>2</sub>. Reproduced with permission from reference [223]. Copyright 2016 American Chemical Society. (B) Schematic representation of the synthetic procedure employed for the preparation of MoS<sub>2</sub>@N-GQDs-IL. Reproduced with permission from reference [183]. Copyright 2021 Elsevier.

## 7. Conclusions and Perspectives

The combination of graphene quantum dots (GQDs) with other materials has been shown to be a potential strategy for developing electrochemical sensors with excellent performances towards the detection of several analytes. The main contributing factor can be ascribed to the synergistic effect that improves the performance of the electrochemical sensing devices. Specifically, here we addressed the main routes to obtain GQDs-based nanocomposites and illustrated results using such composite materials in varied elec-

trochemical sensors. In this regard, Figure 9 shows that 0D nanomaterials are the most common type of materials combined with GQDs for electrochemical sensors. In this sense, metal and metal oxide nanoparticles are the most frequently used materials. Comparatively, the combination with 1D and 2D nanostructures, despite having good performances, is still very inferior when compared to 0D nanomaterials. Thus, works reporting these combinations are expected to increase considerably in the coming years. In addition to these structures, GQDs have also been frequently combined with different platforms not fitted in this classification (other types) to achieve a good performance in specific electrochemical sensing applications. A major part of the works using GQDs-based nanomaterials, however, uses more than one type of material (23.8%).

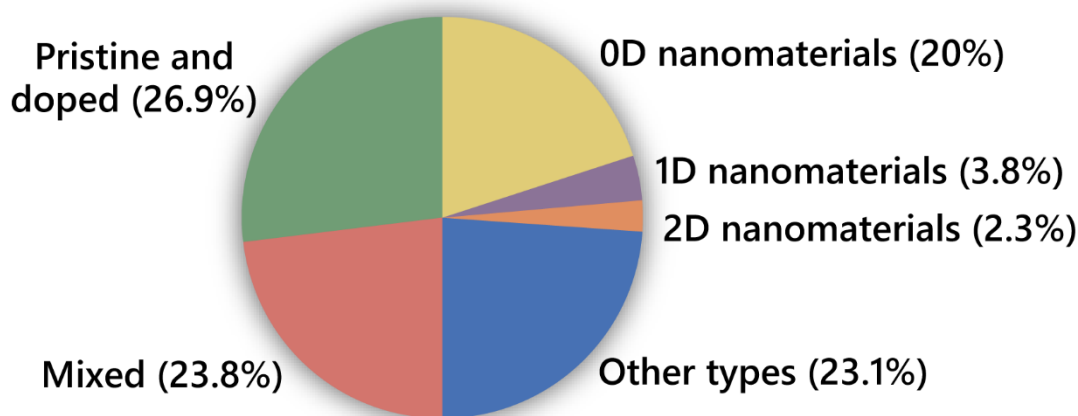


**Figure 9.** Distribution of the published articles (around 150) according to the different materials used to obtain the GQDs-based electrochemical sensors. Data obtained from Web of Science accessed in June 2021 using the keywords “graphene quantum dots” and “electrochemical sensors”.

Electrochemiluminescent sensors using GQDs-based nanocomposites are still poorly reported, as well as the use of GQDs acting as a nanozyme combined with other materials. In this regard, such fields will certainly be more intensely explored in the near future with potential gains in terms of sensor performance. Besides, the portability of electrochemical sensor devices for in situ measurements can be considered as the next major advance to be conquered. In this scenario, the use of nanocomposites represents a promising alternative for the miniaturization and portability of such devices, and GQDs will certainly have a prominent role in this accomplishment.

**Author Contributions:** Conceptualization, M.H.M.F., L.A.M. and D.S.C.; methodology, M.H.M.F., L.A.M. and D.S.C.; resources, D.S.C.; writing—original draft preparation, M.H.M.F., R.S., J.B.S.L. and L.A.M.; writing—review and editing, D.S.C.; supervision, D.S.C. All authors have read and agreed to the published version of the manuscript.

**Funding:** The authors thank the financial support from FAPESP (2018/22214-6, 2017/10582-8, 2018/18468-2), CNPq, MCTI-SisNano (CNPq/402.287/2013-4), and Rede Agronano (EMBRAPA).

**Institutional Review Board Statement:** Not applicable.

**Informed Consent Statement:** Not applicable.

**Data Availability Statement:** Data available in a publicly accessible repository.

**Conflicts of Interest:** The authors declare no conflict of interest.

## References

1. Novoselov, K.S.; Geim, A.K.; Morozov, S.V.; Jiang, D.; Zhang, Y.; Dubonos, S.V.; Grigorieva, I.V.; Firsov, A.A. Electric Field Effect in Atomically Thin Carbon Films. *Science* **2004**, *306*, 666–669. [[CrossRef](#)]
2. Novoselov, K.S.; Jiang, D.; Schedin, F.; Booth, T.J.; Khotkevich, V.V.; Morozov, S.V.; Geim, A.K. Two-dimensional atomic crystals. *Proc. Natl. Acad. Sci. USA* **2005**, *102*, 10451–10453. [[CrossRef](#)]
3. Novoselov, K.S.; Fal'ko, V.I.; Colombo, L.; Gellert, P.R.; Schwab, M.G.; Kim, K. A roadmap for graphene. *Nature* **2012**, *490*, 192–200. [[CrossRef](#)]
4. Geim, A.K.; Novoselov, K.S. The rise of graphene. *Nat. Mater.* **2007**, *6*, 183–191. [[CrossRef](#)]
5. Compton, O.C.; Nguyen, S.T. Graphene oxide, highly reduced graphene oxide, and graphene: Versatile building blocks for carbon-based materials. *Small* **2010**, *6*, 711–723. [[CrossRef](#)]
6. Mao, S.; Pu, H.; Chen, J. Graphene oxide and its reduction: Modeling and experimental progress. *RSC Adv.* **2012**, *2*, 2643–2662. [[CrossRef](#)]
7. Ponomarenko, L.A.; Schedin, F.; Katsnelson, M.I.; Yang, R.; Hill, E.W.; Novoselov, K.S.; Geim, A.K. Chaotic Dirac Billiard in Graphene Quantum Dots. *Science* **2008**, *320*, 356–358. [[CrossRef](#)] [[PubMed](#)]
8. Facure, M.H.M.; Schneider, R.; Mercante, L.A.; Correa, D.S. A review on graphene quantum dots and their nanocomposites: From laboratory synthesis towards agricultural and environmental applications. *Environ. Sci. Nano* **2020**, *7*, 3710–3734. [[CrossRef](#)]
9. Yan, Y.; Gong, J.; Chen, J.; Zeng, Z.; Huang, W.; Pu, K.; Liu, J.; Chen, P. Recent Advances on Graphene Quantum Dots: From Chemistry and Physics to Applications. *Adv. Mater.* **2019**, *31*, 1808283. [[CrossRef](#)] [[PubMed](#)]
10. Shen, J.; Zhu, Y.; Yang, X.; Li, C. Graphene quantum dots: Emergent nanolights for bioimaging, sensors, catalysis and photovoltaic devices. *Chem. Commun.* **2012**, *48*, 3686–3699. [[CrossRef](#)]
11. Haque, E.; Kim, J.; Malgras, V.; Reddy, K.R.; Ward, A.C.; You, J.; Bando, Y.; Hossain, M.S.A.; Yamauchi, Y. Recent Advances in Graphene Quantum Dots: Synthesis, Properties, and Applications. *Small Methods* **2018**, *2*, 1800050. [[CrossRef](#)]
12. Tian, P.; Tang, L.; Teng, K.S.; Lau, S.P. Graphene quantum dots from chemistry to applications. *Mater. Today Chem.* **2018**, *10*, 221–258. [[CrossRef](#)]
13. Choudhary, R.P.; Shukla, S.; Vaibhav, K.; Pawar, P.B.; Saxena, S. Optical properties of few layered graphene quantum dots. *Mater. Res. Express* **2015**, *2*, 95024. [[CrossRef](#)]
14. Jin, S.H.; Kim, D.H.; Jun, G.H.; Hong, S.H.; Jeon, S. Tuning the Photoluminescence of Graphene Quantum Dots through the Charge Transfer Effect of Functional Groups. *ACS Nano* **2013**, *7*, 1239–1245. [[CrossRef](#)] [[PubMed](#)]
15. Ye, R.; Peng, Z.; Metzger, A.; Lin, J.; Mann, J.A.; Huang, K.; Xiang, C.; Fan, X.; Samuel, E.L.G.; Alemany, L.B.; et al. Bandgap Engineering of Coal-Derived Graphene Quantum Dots. *ACS Appl. Mater. Interfaces* **2015**, *7*, 7041–7048. [[CrossRef](#)] [[PubMed](#)]
16. Abdelsalam, H.; Elhaes, H.; Ibrahim, M.A. Tuning electronic properties in graphene quantum dots by chemical functionalization: Density functional theory calculations. *Chem. Phys. Lett.* **2018**, *695*, 138–148. [[CrossRef](#)]
17. Lim, C.S.; Hola, K.; Ambrosi, A.; Zboril, R.; Pumera, M. Graphene and carbon quantum dots electrochemistry. *Electrochem. Commun.* **2015**, *52*, 75–79. [[CrossRef](#)]
18. Faridbod, F.; Sanati, A.L. Graphene Quantum Dots in Electrochemical Sensors/Biosensors. *Curr. Anal. Chem.* **2019**, *15*, 103–123. [[CrossRef](#)]
19. Campuzano, S.; Yáñez-Sedeño, P.; Pingarrón, J.M. Carbon Dots and Graphene Quantum Dots in Electrochemical Biosensing. *Nanomaterials* **2019**, *9*, 634. [[CrossRef](#)]
20. Pumera, M.; Ambrosi, A.; Bonanni, A.; Chng, E.L.K.; Poh, H.L. Graphene for electrochemical sensing and biosensing. *TrAC Trends Anal. Chem.* **2010**, *29*, 954–965. [[CrossRef](#)]
21. Stetter, J.R.; Penrose, W.R.; Yao, S. Sensors, Chemical Sensors, Electrochemical Sensors, and ECS. *J. Electrochem. Soc.* **2003**, *150*, S11. [[CrossRef](#)]
22. Wu, S.; He, Q.; Tan, C.; Wang, Y.; Zhang, H. Graphene-Based Electrochemical Sensors. *Small* **2013**, *9*, 1160–1172. [[CrossRef](#)]
23. Asadian, E.; Ghalkhani, M.; Shahrokhan, S. Electrochemical sensing based on carbon nanoparticles: A review. *Sens. Actuators B Chem.* **2019**, *293*, 183–209. [[CrossRef](#)]
24. Jadon, N.; Jain, R.; Sharma, S.; Singh, K. Recent trends in electrochemical sensors for multianalyte detection—A review. *Talanta* **2016**, *161*, 894–916. [[CrossRef](#)]
25. Benítez-Martínez, S.; Valcárcel, M. Graphene quantum dots in analytical science. *Trends Anal. Chem.* **2015**, *72*, 93–113. [[CrossRef](#)]
26. Sun, H.; Wu, L.; Wei, W.; Qu, X. Recent advances in graphene quantum dots for sensing. *Mater. Today* **2013**, *16*, 433–442. [[CrossRef](#)]
27. Xie, R.; Wang, Z.; Zhou, W.; Liu, Y.; Fan, L.; Li, Y.; Li, X. Graphene quantum dots as smart probes for biosensing. *Anal. Methods* **2016**, *8*, 4001–4006. [[CrossRef](#)]
28. Jie, G.; Zhou, Q.; Jie, G. Graphene quantum dots-based electrochemiluminescence detection of DNA using multiple cycling amplification strategy. *Talanta* **2019**, *194*, 658–663. [[CrossRef](#)] [[PubMed](#)]
29. Zhang, R.; Adsetts, J.R.; Nie, Y.; Sun, X.; Ding, Z. Electrochemiluminescence of nitrogen- and sulfur-doped graphene quantum dots. *Carbon N. Y.* **2018**, *129*, 45–53. [[CrossRef](#)]
30. Zhang, Y.; Wu, C.; Zhou, X.; Wu, X.; Yang, Y.; Wu, H.; Guo, S.; Zhang, J. Graphene quantum dots/gold electrode and its application in living cell H<sub>2</sub>O<sub>2</sub> detection. *Nanoscale* **2013**, *5*, 1816–1819. [[CrossRef](#)]
31. Zheng, A.-X.; Cong, Z.-X.; Wang, J.-R.; Li, J.; Yang, H.-H.; Chen, G.-N. Highly-efficient peroxidase-like catalytic activity of graphene dots for biosensing. *Biosens. Bioelectron.* **2013**, *49*, 519–524. [[CrossRef](#)]

32. Nirala, N.R.; Khandelwal, G.; Kumar, B.; Vinita; Prakash, R.; Kumar, V. One step electro-oxidative preparation of graphene quantum dots from wood charcoal as a peroxidase mimetic. *Talanta* **2017**, *173*, 36–43. [[CrossRef](#)] [[PubMed](#)]
33. Nirala, N.R.; Abraham, S.; Kumar, V.; Bansal, A.; Srivastava, A.; Saxena, P.S. Colorimetric detection of cholesterol based on highly efficient peroxidase mimetic activity of graphene quantum dots. *Sens. Actuators B Chem.* **2015**, *218*, 42–50. [[CrossRef](#)]
34. Ballesteros, C.A.S.; Mercante, L.; Alvarenga, A.; Moreira Facure, M.H.; Schneider, R.; Correa, D. Recent trends in nanozymes design: From materials and structures to environmental applications. *Mater. Chem. Front.* **2021**. [[CrossRef](#)]
35. Sun, H.; Zhou, Y.; Ren, J.; Qu, X. Carbon Nanozymes: Enzymatic Properties, Catalytic Mechanism, and Applications. *Angew. Chem. Int. Ed.* **2018**, *57*, 9224–9237. [[CrossRef](#)]
36. Sun, H.; Ren, J.; Qu, X. Carbon-based Nanozymes BT—Nanozymology: Connecting Biology and Nanotechnology. In *Nanozymology*; Yan, X., Ed.; Springer: Singapore, 2020; pp. 171–193. ISBN 978-981-15-1490-6.
37. Garg, B.; Bisht, T. Carbon Nanodots as Peroxidase Nanozymes for Biosensing. *Molecules* **2016**, *21*, 1653. [[CrossRef](#)]
38. Chen, W.; Lv, G.; Hu, W.; Li, D.; Chen, S.; Dai, Z. Synthesis and applications of graphene quantum dots: A review. *Nanotechnol. Rev.* **2018**, *7*, 157–185. [[CrossRef](#)]
39. Kundu, S.; Pillai, V.K. Synthesis and characterization of graphene quantum dots. *Phys. Sci. Rev.* **2019**, *5*, 1–35. [[CrossRef](#)]
40. Ozhukil Valappil, M.; Pillai, V.K.; Alwarappan, S. Spotlighting graphene quantum dots and beyond: Synthesis, properties and sensing applications. *Appl. Mater. Today* **2017**, *9*, 350–371. [[CrossRef](#)]
41. Bacon, M.; Bradley, S.J.; Nann, T. Graphene quantum dots. *Part. Syst. Charact.* **2014**, *31*, 415–428. [[CrossRef](#)]
42. Li, M.; Chen, T.; Gooding, J.J.; Liu, J. Review of carbon and graphene quantum dots for sensing. *ACS Sens.* **2019**, *4*, 1732–1748. [[CrossRef](#)]
43. Asadi, E.; Fassadi Chimeh, A.; Hosseini, S.; Rahimi, S.; Sarkhosh, B.; Bazli, L.; Bashiri, R.; Vakili Tahmorsati, A.H. A Review of Clinical Applications of Graphene Quantum Dot-based Composites. *J. Compos. Compd.* **2019**, *1*, 36–47. [[CrossRef](#)]
44. Zheng, X.T.; Ananthanarayanan, A.; Luo, K.Q.; Chen, P. Glowing graphene quantum dots and carbon dots: Properties, syntheses, and biological applications. *Small* **2015**, *11*, 1620–1636. [[CrossRef](#)]
45. Liu, W.; Li, M.; Jiang, G.; Li, G.; Zhu, J.; Xiao, M.; Zhu, Y.; Gao, R.; Yu, A.; Feng, M.; et al. Graphene Quantum Dots-Based Advanced Electrode Materials: Design, Synthesis and Their Applications in Electrochemical Energy Storage and Electrocatalysis. *Adv. Energy Mater.* **2020**, *10*, 2001275. [[CrossRef](#)]
46. Sun, H.; Ji, H.; Ju, E.; Guan, Y.; Ren, J.; Qu, X. Synthesis of Fluorinated and Nonfluorinated Graphene Quantum Dots through a New Top-Down Strategy for Long-Time Cellular Imaging. *Chem. Eur. J.* **2015**, *21*, 3791–3797. [[CrossRef](#)]
47. Zhu, X.; Zuo, X.; Hu, R.; Xiao, X.; Liang, Y.; Nan, J. Hydrothermal synthesis of two photoluminescent nitrogen-doped graphene quantum dots emitted green and khaki luminescence. *Mater. Chem. Phys.* **2014**, *147*, 963–967. [[CrossRef](#)]
48. Sun, Y.; Wang, S.; Li, C.; Luo, P.; Tao, L.; Wei, Y.; Shi, G. Large scale preparation of graphene quantum dots from graphite with tunable fluorescence properties. *Phys. Chem. Chem. Phys.* **2013**, *15*, 9907–9913. [[CrossRef](#)] [[PubMed](#)]
49. Chen, W.; Li, F.; Wu, C.; Guo, T. Optical properties of fluorescent zigzag graphene quantum dots derived from multi-walled carbon nanotubes. *Appl. Phys. Lett.* **2014**, *104*, 63109. [[CrossRef](#)]
50. Peng, J.; Gao, W.; Gupta, B.K.; Liu, Z.; Romero-Aburto, R.; Ge, L.; Song, L.; Alemany, L.B.; Zhan, X.; Gao, G.; et al. Graphene Quantum Dots Derived from Carbon Fibers. *Nano Lett.* **2012**, *12*, 844–849. [[CrossRef](#)] [[PubMed](#)]
51. Chen, A.; Zhao, C.; Yu, Y.; Yang, J. Graphene quantum dots derived from carbon fibers for oxidation of dopamine. *J. Wuhan Univ. Technol. Sci. Ed.* **2016**, *31*, 1294–1297. [[CrossRef](#)]
52. Pan, D.; Guo, L.; Zhang, J.; Xi, C.; Xue, Q.; Huang, H.; Li, J.; Zhang, Z.; Yu, W.; Chen, Z.; et al. Cutting sp<sup>2</sup> clusters in graphene sheets into colloidal graphene quantum dots with strong green fluorescence. *J. Mater. Chem.* **2012**, *22*, 3314–3318. [[CrossRef](#)]
53. He, M.; Guo, X.; Huang, J.; Shen, H.; Zeng, Q.; Wang, L. Mass production of tunable multicolor graphene quantum dots from an energy resource of coke by a one-step electrochemical exfoliation. *Carbon N. Y.* **2018**, *140*, 508–520. [[CrossRef](#)]
54. Chu, K.; Adsetts, J.R.; He, S.; Zhan, Z.; Yang, L.; Wong, J.M.; Love, D.A.; Ding, Z. Electrogenerated Chemiluminescence and Electroluminescence of N-Doped Graphene Quantum Dots Fabricated from an Electrochemical Exfoliation Process in Nitrogen-Containing Electrolytes. *Chem. Eur. J.* **2020**, *26*, 15892–15900. [[CrossRef](#)]
55. Pan, D.; Zhang, J.; Li, Z.; Wu, M. Hydrothermal route for cutting graphene sheets into blue-luminescent graphene quantum dots. *Adv. Mater.* **2010**, *22*, 734–738. [[CrossRef](#)]
56. Zhu, Y.; Wang, G.; Jiang, H.; Chen, L.; Zhang, X. One-step ultrasonic synthesis of graphene quantum dots with high quantum yield and their application in sensing alkaline phosphatase. *Chem. Commun.* **2015**, *51*, 948–951. [[CrossRef](#)]
57. Zhang, C.; Cui, Y.; Song, L.; Liu, X.; Hu, Z. Microwave assisted one-pot synthesis of graphene quantum dots as highly sensitive fluorescent probes for detection of iron ions and pH value. *Talanta* **2016**, *150*, 54–60. [[CrossRef](#)]
58. Li, L.-L.; Ji, J.; Fei, R.; Wang, C.-Z.; Lu, Q.; Zhang, J.-R.; Jiang, L.-P.; Zhu, J.-J. A Facile Microwave Avenue to Electrochemiluminescent Two-Color Graphene Quantum Dots. *Adv. Funct. Mater.* **2012**, *22*, 2971–2979. [[CrossRef](#)]
59. Zhuo, S.; Shao, M.; Lee, S.-T. Upconversion and Downconversion Fluorescent Graphene Quantum Dots: Ultrasonic Preparation and Photocatalysis. *ACS Nano* **2012**, *6*, 1059–1064. [[CrossRef](#)]
60. Zhou, X.; Zhang, Y.; Wang, C.; Wu, X.; Yang, Y.; Zheng, B.; Wu, H.; Guo, S.; Zhang, J. Photo-Fenton Reaction of Graphene Oxide: A New Strategy to Prepare Graphene Quantum Dots for DNA Cleavage. *ACS Nano* **2012**, *6*, 6592–6599. [[CrossRef](#)]

61. Oh, S.D.; Kim, J.; Lee, D.H.; Kim, J.H.; Jang, C.W.; Kim, S.; Choi, S.-H. Structural and optical characteristics of graphene quantum dots size-controlled and well-aligned on a large scale by polystyrene-nanosphere lithography. *J. Phys. D Appl. Phys.* **2015**, *49*, 25308. [[CrossRef](#)]
62. Wang, S.; Chen, Z.G.; Cole, I.; Li, Q. Structural evolution of graphene quantum dots during thermal decomposition of citric acid and the corresponding photoluminescence. *Carbon N. Y.* **2015**, *82*, 304–313. [[CrossRef](#)]
63. Alizadeh, T.; Shokri, M. A new humidity sensor based upon graphene quantum dots prepared via carbonization of citric acid. *Sens. Actuators B Chem.* **2016**, *222*, 728–734. [[CrossRef](#)]
64. Wu, X.; Tian, F.; Wang, W.; Chen, J.; Wu, M.; Zhao, J.X. Fabrication of highly fluorescent graphene quantum dots using l-glutamic acid for in vitro/in vivo imaging and sensing. *J. Mater. Chem. C* **2013**, *1*, 4676–4684. [[CrossRef](#)] [[PubMed](#)]
65. Hallaj, T.; Amjadi, M.; Manzoori, J.L.; Shokri, R. Chemiluminescence reaction of glucose-derived graphene quantum dots with hypochlorite, and its application to the determination of free chlorine. *Microchim. Acta* **2015**, *182*, 789–796. [[CrossRef](#)]
66. Shehab, M.; Ebrahim, S.; Soliman, M. Graphene quantum dots prepared from glucose as optical sensor for glucose. *J. Lumin.* **2017**, *184*, 110–116. [[CrossRef](#)]
67. Zhou, L.; Geng, J.; Liu, B. Graphene Quantum Dots from Polycyclic Aromatic Hydrocarbon for Bioimaging and Sensing of Fe<sup>3+</sup> and Hydrogen Peroxide. *Part. Syst. Character.* **2013**, *30*, 1086–1092. [[CrossRef](#)]
68. Chua, C.K.; Sofer, Z.; Šimek, P.; Jankovský, O.; Klímová, K.; Bakardjieva, S.; Hrdličková Kučková, Š.; Pumera, M. Synthesis of Strongly Fluorescent Graphene Quantum Dots by Cage-Opening Buckminsterfullerene. *ACS Nano* **2015**, *9*, 2548–2555. [[CrossRef](#)]
69. Kaciulis, S.; Mezzi, A.; Soltani, P.; Pizzoferrato, R.; Ciotta, E.; Proposito, P. Graphene quantum dots obtained by unfolding fullerene. *Thin Solid Films* **2019**, *673*, 19–25. [[CrossRef](#)]
70. Kumar, S.; Aziz, S.K.T.; Girshevitz, O.; Nessim, G.D. One-Step Synthesis of N-Doped Graphene Quantum Dots from Chitosan as a Sole Precursor Using Chemical Vapor Deposition. *J. Phys. Chem. C* **2018**, *122*, 2343–2349. [[CrossRef](#)]
71. Fan, L.; Zhu, M.; Lee, X.; Zhang, R.; Wang, K.; Wei, J.; Zhong, M.; Wu, D.; Zhu, H. Direct Synthesis of Graphene Quantum Dots by Chemical Vapor Deposition. *Part. Syst. Character.* **2013**, *30*, 764–769. [[CrossRef](#)]
72. Gurrappa, I.; Binder, L. Electrodeposition of nanostructured coatings and their characterization—A review. *Sci. Technol. Adv. Mater.* **2008**, *9*, 43001. [[CrossRef](#)]
73. Hasanzadeh, M.; Karimzadeh, A.; Shadjou, N.; Mokhtarzadeh, A.; Bageri, L.; Sadeghi, S.; Mahboob, S. Graphene quantum dots decorated with magnetic nanoparticles: Synthesis, electrodeposition, characterization and application as an electrochemical sensor towards determination of some amino acids at physiological pH. *Mater. Sci. Eng. C* **2016**, *68*, 814–830. [[CrossRef](#)]
74. Tonelli, D.; Scavetta, E.; Gualandi, I. Electrochemical Deposition of Nanomaterials for Electrochemical Sensing. *Sensors* **2019**, *19*, 1186. [[CrossRef](#)]
75. Oviedo, O.A.; Negre, C.F.A.; Mariscal, M.M.; Sánchez, C.G.; Leiva, E.P.M. Underpotential deposition on free nanoparticles: Its meaning and measurement. *Electrochem. Commun.* **2012**, *16*, 1–5. [[CrossRef](#)]
76. Oviedo, O.A.; Vélez, P.; Macagno, V.A.; Leiva, E.P.M. Underpotential deposition: From planar surfaces to nanoparticles. *Surf. Sci.* **2015**, *631*, 23–34. [[CrossRef](#)]
77. Shamsi, A.; Ahour, F.; Sehatnia, B. Nickel oxide nanoparticles decorated graphene quantum dot as an effective electrode modifier for electrocatalytic oxidation and analysis of clozapine. *J. Solid State Electrochem.* **2018**, *22*, 2681–2689. [[CrossRef](#)]
78. Xu, Q.; Yuan, H.; Dong, X.; Zhang, Y.; Asif, M.; Dong, Z.; He, W.; Ren, J.; Sun, Y.; Xiao, F. Dual nanoenzyme modified microelectrode based on carbon fiber coated with AuPd alloy nanoparticles decorated graphene quantum dots assembly for electrochemical detection in clinic cancer samples. *Biosens. Bioelectron.* **2018**, *107*, 153–162. [[CrossRef](#)]
79. Li, J.; Qu, J.; Yang, R.; Qu, L.; de B. Harrington, P. A Sensitive and Selective Electrochemical Sensor Based on Graphene Quantum Dot/Gold Nanoparticle Nanocomposite Modified Electrode for the Determination of Quercetin in Biological Samples. *Electroanalysis* **2016**, *28*, 1322–1330. [[CrossRef](#)]
80. Andre, R.S.; Mercante, L.A.; Fature, M.H.M.; Pavinatto, A.; Correa, D.S. 8—Electrospun composite nanofibers as sensors for food analysis. *Electrospun Polym. Compos.* **2021**, 261–286. [[CrossRef](#)]
81. Correa, D.S.; Mercante, L.A.; Schneider, R.; Fature, M.H.M.; Locilento, D.A. Composite Nanofibers for Removing Water Pollutants: Fabrication Techniques BT—Handbook of Ecomaterials. In *Handbook of Ecomaterial*; Martínez, L.M.T., Kharissova, O.V., Kharisov, B.I., Eds.; Springer International Publishing: Cham, Switzerland, 2017; pp. 1–29. ISBN 978-3-319-68255-6.
82. Mercante, L.A.; Scagion, V.P.; Migliorini, F.L.; Mattoso, L.H.C.C.; Correa, D.S. Electrospinning-based (bio)sensors for food and agricultural applications: A review. *Trends Anal. Chem.* **2017**, *91*, 91–103. [[CrossRef](#)]
83. Correa, D.S.; Pavinatto, A.; Mercante, L.A.; Mattoso, L.H.C.; Oliveira, J.E.; Riul, A. Chemical sensors based on hybrid nanomaterials for food analysis. *Nanobiosensors* **2017**, 205–244. [[CrossRef](#)]
84. Ray, S.S.; Chen, S.-S.; Li, C.-W.; Nguyen, N.C.; Nguyen, H.T. A comprehensive review: Electrospinning technique for fabrication and surface modification of membranes for water treatment application. *RSC Adv.* **2016**, *6*, 85495–85514. [[CrossRef](#)]
85. Wang, N.; Zhu, Z.; Sheng, J.; Al-Deyab, S.S.; Yu, J.; Ding, B. Superamphiphobic nanofibrous membranes for effective filtration of fine particles. *J. Colloid Interface Sci.* **2014**, *428*, 41–48. [[CrossRef](#)]
86. Wang, G.; Shi, G.; Chen, X.; Yao, R.; Chen, F. A glassy carbon electrode modified with graphene quantum dots and silver nanoparticles for simultaneous determination of guanine and adenine. *Microchim. Acta* **2015**, *182*, 315–322. [[CrossRef](#)]

87. Mahmoudi-Moghaddam, H.; Tajik, S.; Beitollahi, H. A new electrochemical DNA biosensor based on modified carbon paste electrode using graphene quantum dots and ionic liquid for determination of topotecan. *Microchem. J.* **2019**, *150*, 104085. [[CrossRef](#)]
88. Talari, F.F.; Bozorg, A.; Faridbod, F.; Vossoughi, M. A novel sensitive aptamer-based nanosensor using rGQDs and MWCNTs for rapid detection of diazinon pesticide. *J. Environ. Chem. Eng.* **2021**, *9*, 104878. [[CrossRef](#)]
89. Zhang, P.; Zhao, X.; Ji, Y.; Ouyang, Z.; Wen, X.; Li, J.; Su, Z.; Wei, G. Electrospinning graphene quantum dots into a nanofibrous membrane for dual-purpose fluorescent and electrochemical biosensors. *J. Mater. Chem. B* **2015**, *3*, 2487–2496. [[CrossRef](#)] [[PubMed](#)]
90. Ye, N.; Yan, T.; Jiang, Z.; Wu, W.; Fang, T. A review: Conventional and supercritical hydro/solvothermal synthesis of ultrafine particles as cathode in lithium battery. *Ceram. Int.* **2018**, *44*, 4521–4537. [[CrossRef](#)]
91. Feng, S.-H.; Li, G.-H. Hydrothermal and Solvothermal Syntheses. In *Modern Inorganic Synthetic Chemistry*, 2nd ed.; Xu, R., Xu, Y.B.T., Eds.; Elsevier: Amsterdam, The Netherlands, 2017; Chapter 4; pp. 73–104. ISBN 978-0-444-63591-4.
92. Tetsuka, H.; Asahi, R.; Nagoya, A.; Okamoto, K.; Tajima, I.; Ohta, R.; Okamoto, A. Optically tunable amino-functionalized graphene quantum dots. *Adv. Mater.* **2012**, *24*, 5333–5338. [[CrossRef](#)]
93. Emran, M.Y.; Shenashen, M.A.; Abdelwahab, A.A.; Abdelmottaleb, M.; El-Safty, S.A. Facile synthesis of microporous sulfur-doped carbon spheres as electrodes for ultrasensitive detection of ascorbic acid in food and pharmaceutical products. *New J. Chem.* **2018**, *42*, 5037–5044. [[CrossRef](#)]
94. Shen, J.; Zhu, Y.; Yang, X.; Zong, J.; Zhang, J.; Li, C. One-pot hydrothermal synthesis of graphene quantum dots surface-passivated by polyethylene glycol and their photoelectric conversion under near-infrared light. *New J. Chem.* **2012**, *36*, 97–101. [[CrossRef](#)]
95. Liu, Q.; Li, J.; Zhao, Y.; Zhou, Y.; Li, C. CdS nanoparticle-functionalized natural cotton cellulose electrospun nanofibers for visible light photocatalysis. *Mater. Lett.* **2015**, *138*, 89–91. [[CrossRef](#)]
96. Zhang, T.; Gu, Y.; Li, C.; Yan, X.; Lu, N.; Liu, H.; Zhang, Z.; Zhang, H. Fabrication of Novel Electrochemical Biosensor Based on Graphene Nanohybrid to Detect H<sub>2</sub>O<sub>2</sub> Released from Living Cells with Ultrahigh Performance. *ACS Appl. Mater. Interfaces* **2017**, *9*, 37991–37999. [[CrossRef](#)] [[PubMed](#)]
97. Rane, A.V.; Kanny, K.; Abitha, V.K.; Thomas, S. Methods for Synthesis of Nanoparticles and Fabrication of Nanocomposites. In *Micro and Nano Technologies*; Mohan Bhagyaraj, S., Oluwafemi, O.S., Kalarikkal, N., Thomas, S.B.T., Eds.; Woodhead Publishing: Cambridge, UK, 2018; Chapter 5; pp. 121–139. ISBN 978-0-08-101975-7.
98. Babooram, K. 28—Novel solution routes to ferroelectrics and relaxors. In *Handbook of Advanced Dielectric, Piezoelectric and Ferroelectric Materials*; Woodhead Publishing Series in Electronic and Optical Materials; Ye, Z.-G., Ed.; Woodhead Publishing: Cambridge, UK, 2008; pp. 852–883. ISBN 978-1-84569-186-8.
99. Wu, X.; Zhang, Y.; Han, T.; Wu, H.; Guo, S.; Zhang, J. Composite of graphene quantum dots and Fe<sub>3</sub>O<sub>4</sub> nanoparticles: Peroxidase activity and application in phenolic compound removal. *RSC Adv.* **2014**, *4*, 3299–3305. [[CrossRef](#)]
100. Ramachandran, S.; Sathishkumar, M.; Kothurkar, N.K.; Senthilkumar, R. Synthesis and characterization of graphene quantum dots/cobalt ferrite nanocomposite. *IOP Conf. Ser. Mater. Sci. Eng.* **2018**, *310*, 12139. [[CrossRef](#)]
101. Raeyani, D.; Shojaei, S.; Ahmadi-Kandjani, S. Optical graphene quantum dots gas sensors: Experimental study. *Mater. Res. Express* **2020**, *7*, 15608. [[CrossRef](#)]
102. Arunragasa, S.; Seekaew, Y.; Pon-On, W.; Wongchoosuk, C. Hydroxyl edge-functionalized graphene quantum dots for gas-sensing applications. *Diam. Relat. Mater.* **2020**, *105*, 107790. [[CrossRef](#)]
103. Yang, B.; Chen, J.; Cui, L.; Liu, W. Enhanced photocurrent of a ZnO nanorod array sensitized with graphene quantum dots. *RSC Adv.* **2015**, *5*, 59204–59207. [[CrossRef](#)]
104. Kepić, D.P.; Marković, Z.M.; Jovanović, S.P.; Peruško, D.B.; Budimir, M.D.; Holclajtner-Antunović, I.D.; Pavlović, V.B.; Todorović Marković, B.M. Preparation of PEDOT:PSS thin films doped with graphene and graphene quantum dots. *Synth. Met.* **2014**, *198*, 150–154. [[CrossRef](#)]
105. Zeng, Z.; Xiao, F.-X.; Gui, X.; Wang, R.; Liu, B.; Yang Tan, T.T. Layer-by-layer assembly of nitrogen-doped graphene quantum dots monolayer decorated one-dimensional semiconductor nanoarchitectures for solar-driven water splitting. *J. Mater. Chem. A* **2016**, *4*, 16383–16393. [[CrossRef](#)]
106. Hasanzadeh, M.; Mokhtari, F.; Shadjou, N.; Eftekhari, A.; Mokhtarzadeh, A.; Jouyban-Gharamaleki, V.; Mahboob, S. Poly arginine-graphene quantum dots as a biocompatible and non-toxic nanocomposite: Layer-by-layer electrochemical preparation, characterization and non-invasive malondialdehyde sensory application in exhaled breath condensate. *Mater. Sci. Eng. C* **2017**, *75*, 247–258. [[CrossRef](#)]
107. Zeng, Z.; Xiao, F.-X.; Phan, H.; Chen, S.; Yu, Z.; Wang, R.; Nguyen, T.-Q.; Yang Tan, T.T. Unraveling the cooperative synergy of zero-dimensional graphene quantum dots and metal nanocrystals enabled by layer-by-layer assembly. *J. Mater. Chem. A* **2018**, *6*, 1700–1713. [[CrossRef](#)]
108. Xu, S.; Li, F.; Su, B.; Hu, M.Z.; Gao, X.; Gao, C. Novel graphene quantum dots (GQDs)-incorporated thin film composite (TFC) membranes for forward osmosis (FO) desalination. *Desalination* **2019**, *451*, 219–230. [[CrossRef](#)]
109. Rahimi, K.; Yazdani, A.; Ahmadi-rad, M. Graphene quantum dots enhance UV photoresponsivity and surface-related sensing speed of zinc oxide nanorod thin films. *Mater. Des.* **2018**, *140*, 222–230. [[CrossRef](#)]

110. Rojas-Andrade, M.D.; Nguyen, T.A.; Mistler, W.P.; Armas, J.; Lu, J.E.; Roseman, G.; Hollingsworth, W.R.; Nichols, F.; Millhauser, G.L.; Ayzner, A.; et al. Antimicrobial activity of graphene oxide quantum dots: Impacts of chemical reduction. *Nanoscale Adv.* **2020**, *2*, 1074–1083. [[CrossRef](#)]
111. Udayabhaskar, R.; Mangalaraja, R.V.; Pandiyarajan, T.; Karthikeyan, B.; Mansilla, H.D.; Contreras, D. Spectroscopic investigation on graphene-copper nanocomposites with strong UV emission and high catalytic activity. *Carbon N. Y.* **2017**, *124*, 256–262. [[CrossRef](#)]
112. Kadian, S.; Manik, G.; Kalkal, A.; Singh, M.; Chauhan, R.P. Effect of sulfur doping on fluorescence and quantum yield of graphene quantum dots: An experimental and theoretical investigation. *Nanotechnology* **2019**, *30*, 435704. [[CrossRef](#)]
113. Zhu, S.; Shao, J.; Song, Y.; Zhao, X.; Du, J.; Wang, L.; Wang, H.; Zhang, K.; Zhang, J.; Yang, B. Investigating the surface state of graphene quantum dots. *Nanoscale* **2015**, *7*, 7927–7933. [[CrossRef](#)] [[PubMed](#)]
114. Tabish, T.A.; Lin, L.; Ali, M.; Jabeen, F.; Ali, M.; Iqbal, R.; Horsell, D.W.; Winyard, P.G.; Zhang, S. Investigating the bioavailability of graphene quantum dots in lung tissues via Fourier transform infrared spectroscopy. *Interface Focus* **2018**, *8*, 20170054. [[CrossRef](#)]
115. Chhabra, V.A.; Kaur, R.; Kumar, N.; Deep, A.; Rajesh, C.; Kim, K.-H. Synthesis and spectroscopic studies of functionalized graphene quantum dots with diverse fluorescence characteristics. *RSC Adv.* **2018**, *8*, 11446–11454. [[CrossRef](#)]
116. Wu, J.; Wang, P.; Wang, F.; Fang, Y. Investigation of the microstructures of graphene quantum dots (GQDs) by surface-enhanced raman spectroscopy. *Nanomaterials* **2018**, *8*, 864. [[CrossRef](#)]
117. Thang, P.N.; Hung, L.X.; Thuan, D.N.; Yen, N.H.; Hien, N.T.T.; Hanh, V.T.H.; Khang, N.C.; Laverdant, J.; Nga, P.T. Temperature-dependent Raman investigation and photoluminescence of graphene quantum dots with and without nitrogen-doping. *J. Mater. Sci.* **2021**, *56*, 4979–4990. [[CrossRef](#)]
118. Dervishi, E.; Ji, Z.; Htoon, H.; Sykora, M.; Doorn, S.K. Raman spectroscopy of bottom-up synthesized graphene quantum dots: Size and structure dependence. *Nanoscale* **2019**, *11*, 16571–16581. [[CrossRef](#)] [[PubMed](#)]
119. Zhu, S.; Zhang, J.; Liu, X.; Li, B.; Wang, X.; Tang, S.; Meng, Q.; Li, Y.; Shi, C.; Hu, R.; et al. Graphene quantum dots with controllable surface oxidation, tunable fluorescence and up-conversion emission. *RSC Adv.* **2012**, *2*, 2717–2720. [[CrossRef](#)]
120. Wang, Y.; Kong, W.; Wang, L.; Zhang, J.Z.; Li, Y.; Liu, X.; Li, Y. Optimizing oxygen functional groups in graphene quantum dots for improved antioxidant mechanism. *Phys. Chem. Chem. Phys.* **2019**, *21*, 1336–1343. [[CrossRef](#)] [[PubMed](#)]
121. Zhu, S.; Zhang, J.; Tang, S.; Qiao, C.; Wang, L.; Wang, H.; Liu, X.; Li, B.; Li, Y.; Yu, W.; et al. Surface chemistry routes to modulate the photoluminescence of graphene quantum dots: From fluorescence mechanism to up-conversion bioimaging applications. *Adv. Funct. Mater.* **2012**, *22*, 4732–4740. [[CrossRef](#)]
122. Tang, L.; Ji, R.; Cao, X.; Lin, J.; Jiang, H.; Li, X.; Teng, K.S.; Luk, C.M.; Zeng, S.; Hao, J.; et al. Deep ultraviolet photoluminescence of water-soluble self-passivated graphene quantum dots. *ACS Nano* **2012**, *6*, 5102–5110. [[CrossRef](#)]
123. Dejpasand, M.T.; Saievar-Iranizad, E.; Bayat, A.; Montaghemi, A.; Ardekani, S.R. Tuning HOMO and LUMO of three region (UV, Vis and IR) photoluminescent nitrogen doped graphene quantum dots for photodegradation of methylene blue. *Mater. Res. Bull.* **2020**, *128*, 110886. [[CrossRef](#)]
124. Pierrat, P.; Gaumet, J.-J. Graphene quantum dots: Emerging organic materials with remarkable and tunable luminescence features. *Tetrahedron Lett.* **2020**, *61*, 152554. [[CrossRef](#)]
125. Xin, Q.; Shah, H.; Xie, W.; Wang, Y.; Jia, X.; Nawaz, A.; Song, M.; Gong, J.R. Preparation of blue- and green-emissive nitrogen-doped graphene quantum dots from graphite and their application in bioimaging. *Mater. Sci. Eng. C* **2021**, *119*, 111642. [[CrossRef](#)] [[PubMed](#)]
126. Guo, B.; Zuo, Y.; Shi, Y.; Han, T.; Lanza, M. Transmission Electron Microscopy-Based Statistical Analysis of Commercially Available Graphene Oxide Quantum Dots. *Cryst. Res. Technol.* **2020**, *55*, 1900231. [[CrossRef](#)]
127. Wang, G.; Guo, Q.; Chen, D.; Liu, Z.; Zheng, X.; Xu, A.; Yang, S.; Ding, G. Facile and Highly Effective Synthesis of Controllable Lattice Sulfur-Doped Graphene Quantum Dots via Hydrothermal Treatment of Durian. *ACS Appl. Mater. Interfaces* **2018**, *10*, 5750–5759. [[CrossRef](#)]
128. Liu, F.; Jang, M.-H.; Ha, H.D.; Kim, J.-H.; Cho, Y.-H.; Seo, T.S. Facile Synthetic Method for Pristine Graphene Quantum Dots and Graphene Oxide Quantum Dots: Origin of Blue and Green Luminescence. *Adv. Mater.* **2013**, *25*, 3657–3662. [[CrossRef](#)]
129. Ritter, K.A.; Lyding, J.W. The influence of edge structure on the electronic properties of graphene quantum dots and nanoribbons. *Nat. Mater.* **2009**, *8*, 235–242. [[CrossRef](#)]
130. Lu, H.F.; Zhang, M.M.; Wu, D.; Huang, J.L.; Zhu, L.L.; Wang, C.M.; Zhang, Q.L. Colorimetric and fluorescent dual-mode sensing of alkaline phosphatase activity in L-02 cells and its application in living cell imaging based on in-situ growth of silver nanoparticles on graphene quantum dots. *Sens. Actuators B Chem.* **2018**, *258*, 461–469. [[CrossRef](#)]
131. Lee, K.; Lee, H.; Shin, Y.; Yoon, Y.; Kim, D.; Lee, H. Highly transparent and flexible supercapacitors using graphene-graphene quantum dots chelate. *Nano Energy* **2016**, *26*, 746–754. [[CrossRef](#)]
132. Liu, Q.; Sun, J.; Gao, K.; Chen, N.; Sun, X.; Ti, D.; Bai, C.; Cui, R.; Qu, L. Graphene quantum dots for energy storage and conversion: From fabrication to applications. *Mater. Chem. Front.* **2020**, *4*, 421–436. [[CrossRef](#)]
133. Wu, W.; Zhang, J.; Shen, W.; Zhong, M.; Guo, S. Graphene Quantum Dots Band Structure Tuned by Size for Efficient Organic Solar Cells. *Phys. Status Solidi* **2019**, *216*, 1900657. [[CrossRef](#)]
134. Zhang, Z.Z.; Chang, K.; Peeters, F.M. Tuning of energy levels and optical properties of graphene quantum dots. *Phys. Rev. B Condens. Matter Mater. Phys.* **2008**, *77*, 235411. [[CrossRef](#)]

135. Cai, J.; Ruffieux, P.; Jaafar, R.; Bieri, M.; Braun, T.; Blankenburg, S.; Muoth, M.; Seitsonen, A.P.; Saleh, M.; Feng, X.; et al. Atomically precise bottom-up fabrication of graphene nanoribbons. *Nature* **2010**, *466*, 470–473. [[CrossRef](#)]
136. Ruffieux, P.; Wang, S.; Yang, B.; Sanchez-Sanchez, C.; Liu, J.; Dienel, T.; Talirz, L.; Shinde, P.; Pignedoli, C.A.; Passerone, D.; et al. On-surface synthesis of graphene nanoribbons with zigzag edge topology. *Nature* **2016**, *531*, 489–492. [[CrossRef](#)]
137. Tamura, N.; Tomai, T.; Oka, N.; Honma, I. Capacity improvement of the carbon-based electrochemical capacitor by zigzag-edge introduced graphene. *Appl. Surf. Sci.* **2018**, *428*, 986–989. [[CrossRef](#)]
138. Basak, T.; Basak, T. Theoretical investigation of electronic and optical properties of nitrogen doped triangular shaped graphene quantum dots. *J. Phys. Condens. Matter* **2020**, *32*. [[CrossRef](#)] [[PubMed](#)]
139. Ji, Z.; Dervishi, E.; Doorn, S.K.; Sykora, M. Size-Dependent Electronic Properties of Uniform Ensembles of Strongly Confined Graphene Quantum Dots. *J. Phys. Chem. Lett.* **2019**, *10*, 953–959. [[CrossRef](#)]
140. Ramana, L.N.; Dinh, L.N.M.; Agarwal, V. Influence of surface charge of graphene quantum dots on their uptake and clearance in melanoma cells. *Nanoscale Adv.* **2021**. [[CrossRef](#)]
141. Zhao, L.; Duan, G.; Yang, Z.; Weber, J.K.; Liu, X.; Lu, S.; Meng, X.; Xu, J.Y. Particle Size-Dependent Antibacterial Activity and Murine Cell Cytotoxicity Induced by Graphene Oxide Nanomaterials. *J. Nanomater.* **2016**, *2016*, 6709764. [[CrossRef](#)]
142. Deng, D.; Yu, L.; Pan, X.; Wang, S.; Chen, X.; Hu, P.; Sun, L.; Bao, X. Size effect of graphene on electrocatalytic activation of oxygen. *Chem. Commun.* **2011**, *47*, 10016. [[CrossRef](#)]
143. Liu, Y.; Wang, R.; Lang, J.; Yan, X. Insight into the formation mechanism of graphene quantum dots and the size effect on their electrochemical behaviors. *Phys. Chem. Chem. Phys.* **2015**, *17*, 14028–14035. [[CrossRef](#)]
144. Ma, Z.; Sa, R.; Li, Q.; Wu, K. Interfacial electronic structure and charge transfer of hybrid graphene quantum dot and graphitic carbon nitride nanocomposites: Insights into high efficiency for photocatalytic solar water splitting. *Phys. Chem. Chem. Phys.* **2015**, *18*, 1050–1058. [[CrossRef](#)]
145. Xu, H.; Zhang, L.; Ding, Z.; Hu, J.; Liu, J.; Liu, Y. Edge-functionalized graphene quantum dots as a thickness-insensitive cathode interlayer for polymer solar cells. *Nano Res.* **2018**, *11*, 4293–4301. [[CrossRef](#)]
146. Sheely, A.; Gifford, B.; Tretiak, S.; Bishop, A. Tunable Optical Features of Graphene Quantum Dots from Edge Functionalization. *J. Phys. Chem. C* **2021**, *125*, 9244–9252. [[CrossRef](#)]
147. Sun, J.; Yang, S.; Wang, Z.; Shen, H.; Xu, T.; Sun, L.; Li, H.; Chen, W.; Jiang, X.; Ding, G.; et al. Ultra-High Quantum Yield of Graphene Quantum Dots: Aromatic-Nitrogen Doping and Photoluminescence Mechanism. *Part. Syst. Charact.* **2015**, *32*, 434–440. [[CrossRef](#)]
148. Sk, M.A.; Ananthanarayanan, A.; Huang, L.; Lim, K.H.; Chen, P. Revealing the tunable photoluminescence properties of graphene quantum dots. *J. Mater. Chem. C* **2014**, *2*, 6954–6960. [[CrossRef](#)]
149. Kim, J.; Suh, J.S. Size-Controllable and Low-Cost Fabrication of Graphene Quantum Dots Using Thermal Plasma Jet. *ACS Nano* **2014**, *8*, 4190–4196. [[CrossRef](#)] [[PubMed](#)]
150. Bressi, V.; Ferlazzo, A.; Iannazzo, D.; Espro, C. Graphene quantum dots by eco-friendly green synthesis for electrochemical sensing: Recent advances and future perspectives. *Nanomaterials* **2021**, *11*, 1120. [[CrossRef](#)] [[PubMed](#)]
151. Karimzadeh, A.; Hasanzadeh, M.; Shadjou, N.; Guardia, M. de la Electrochemical biosensing using N-GQDs: Recent advances in analytical approach. *TrAC Trends Anal. Chem.* **2018**, *105*, 484–491. [[CrossRef](#)]
152. Tufa, L.T.; Oh, S.; Tran, V.T.; Kim, J.; Jeong, K.J.; Park, T.J.; Kim, H.J.; Lee, J. Electrochemical immunosensor using nanotriplex of graphene quantum dots, Fe<sub>3</sub>O<sub>4</sub> and Ag nanoparticles for tuberculosis. *Electrochim. Acta* **2018**, *290*, 369–377. [[CrossRef](#)]
153. Roushani, M.; Jalilian, Z.; Nezhadali, A. Screen printed carbon electrode sensor with thiol graphene quantum dots and gold nanoparticles for voltammetric determination of solatol. *Heliyon* **2019**, *5*, e01984. [[CrossRef](#)]
154. Fajardo, A.; Tapia, D.; Pizarro, J.; Segura, R.; Jara, P. Determination of norepinephrine using a glassy carbon electrode modified with graphene quantum dots and gold nanoparticles by square wave stripping voltammetry. *J. Appl. Electrochem.* **2019**, *49*, 423–432. [[CrossRef](#)]
155. Arumugasamy, S.K.; Govindaraju, S.; Yun, K. Electrochemical sensor for detecting dopamine using graphene quantum dots incorporated with multiwall carbon nanotubes. *Appl. Surf. Sci.* **2020**, *508*, 145294. [[CrossRef](#)]
156. Huang, Q.; Lin, X.; Tong, L.; Tong, Q.X. Graphene Quantum Dots/Multiwalled Carbon Nanotubes Composite-Based Electrochemical Sensor for Detecting Dopamine Release from Living Cells. *ACS Sustain. Chem. Eng.* **2020**, *8*, 1644–1650. [[CrossRef](#)]
157. Samuei, S.; Fakkar, J.; Rezvani, Z.; Shomali, A.; Habibi, B. Synthesis and characterization of graphene quantum dots/CoNiAl-layered double-hydroxide nanocomposite: Application as a glucose sensor. *Anal. Biochem.* **2017**, *521*, 31–39. [[CrossRef](#)]
158. Chen, Y.C.; Chiang, W.H.; Kurniawan, D.; Yeh, P.C.; Otake, K.I.; Kung, C.W. Impregnation of Graphene Quantum Dots into a Metal-Organic Framework to Render Increased Electrical Conductivity and Activity for Electrochemical Sensing. *ACS Appl. Mater. Interfaces* **2019**, *11*, 35319–35326. [[CrossRef](#)]
159. Hatamluyi, B.; Rezaei, M.; Beheshti, H.R.; Boroushaki, M.T. Ultra-sensitive molecularly imprinted electrochemical sensor for patulin detection based on a novel assembling strategy using Au@Cu-MOF/N-GQDs. *Sens. Actuators B Chem.* **2020**, *318*, 128219. [[CrossRef](#)]
160. Bali Prasad, B.; Kumar, A.; Singh, R. Synthesis of novel monomeric graphene quantum dots and corresponding nanocomposite with molecularly imprinted polymer for electrochemical detection of an anticancerous ifosfamide drug. *Biosens. Bioelectron.* **2017**, *94*, 1–9. [[CrossRef](#)] [[PubMed](#)]

161. Mahmoud, A.M.; El-Wekil, M.M.; Mahnashi, M.H.; Ali, M.F.B.; Alkahtani, S.A. Modification of N,S co-doped graphene quantum dots with p-aminothiophenol-functionalized gold nanoparticles for molecular imprint-based voltammetric determination of the antiviral drug sofosbuvir. *Microchim. Acta* **2019**, *186*, 617. [[CrossRef](#)]
162. Sanati, A.L.; Faridbod, F.; Ganjali, M.R. Synergic effect of graphene quantum dots and room temperature ionic liquid for the fabrication of highly sensitive voltammetric sensor for levodopa determination in the presence of serotonin. *J. Mol. Liq.* **2017**, *241*, 316–320. [[CrossRef](#)]
163. Kunpatee, K.; Traipop, S.; Chailapakul, O.; Chuanuwatanakul, S. Simultaneous determination of ascorbic acid, dopamine, and uric acid using graphene quantum dots/ionic liquid modified screen-printed carbon electrode. *Sens. Actuators B Chem.* **2020**, *314*, 128059. [[CrossRef](#)]
164. Tang, J.; Huang, R.; Zheng, S.; Jiang, S.; Yu, H.; Li, Z.; Wang, J. A sensitive and selective electrochemical sensor based on graphene quantum dots/gold nanoparticles nanocomposite modified electrode for the determination of luteolin in peanut hulls. *Microchem. J.* **2019**, *145*, 899–907. [[CrossRef](#)]
165. Zhou, Z.; Zhao, P.; Wang, C.; Yang, P.; Xie, Y.; Fei, J. Ultra-sensitive amperometric determination of quercetin by using a glassy carbon electrode modified with a nanocomposite prepared from aminated graphene quantum dots, thiolated  $\beta$ -cyclodextrin and gold nanoparticles. *Microchim. Acta* **2020**, *187*. [[CrossRef](#)] [[PubMed](#)]
166. Shamsi, A.; Ahour, F. Electrochemical Sensing of Thioridazine in Human Serum Samples Using Modified Glassy Carbon Electrode. *Adv. J. Chem. A* **2020**, *4*, 22–31.
167. Mansuriya, B.D.; Altintas, Z. Enzyme-free electrochemical nano-immunosensor based on graphene quantum dots and gold nanoparticles for cardiac biomarker determination. *Nanomaterials* **2021**, *11*, 578. [[CrossRef](#)] [[PubMed](#)]
168. Yao, J.; Li, Y.; Xie, M.; Yang, Q.; Liu, T. The electrochemical behaviors and kinetics of AuNPs/N, S-GQDs composite electrode: A novel label-free amplified BPA aptasensor with extreme sensitivity and selectivity. *J. Mol. Liq.* **2020**, *320*, 114384. [[CrossRef](#)]
169. Ahmadi, N.; Bagherzadeh, M.; Nemati, A. Comparison between electrochemical and photoelectrochemical detection of dopamine based on titania-ceria-graphene quantum dots nanocomposite. *Biosens. Bioelectron.* **2020**, *151*, 111977. [[CrossRef](#)]
170. Trinadh, T.; Khuntia, H.; Anusha, T.; Bhavani, K.S.; Kumar, J.V.S.; Brahman, P.K. Synthesis and characterization of nanocomposite material based on graphene quantum dots and lanthanum doped zirconia nanoparticles: An electrochemical sensing application towards flutamide in urine samples. *Diam. Relat. Mater.* **2020**, *110*, 108143. [[CrossRef](#)]
171. Bhardwaj, H.; Pandey, M.K.; Rajesh; Sumana, G. Electrochemical Aflatoxin B1 immunosensor based on the use of graphene quantum dots and gold nanoparticles. *Microchim. Acta* **2019**, *186*, 592. [[CrossRef](#)]
172. Li, L.; Liu, D.; Wang, K.; Mao, H.; You, T. Quantitative detection of nitrite with N-doped graphene quantum dots decorated N-doped carbon nanofibers composite-based electrochemical sensor. *Sens. Actuators B Chem.* **2017**, *252*, 17–23. [[CrossRef](#)]
173. Wu, M.; Zhu, J.; Ren, Y.; Yang, N.; Hong, Y.; Wang, W.; Huang, W.; Si, W.; Dong, X. NH<sub>2</sub>-GQDs-Doped Nickel-Cobalt Oxide Deposited on Carbon Cloth for Nonenzymatic Detection of Glucose. *Adv. Mater. Interfaces* **2020**, *7*, 2–7. [[CrossRef](#)]
174. Mishra, P.; Bhat, B.R. A study on the electro-reductive cycle of amino-functionalized graphene quantum dots immobilized on graphene oxide for amperometric determination of oxalic acid. *Microchim. Acta* **2019**, *186*, 646. [[CrossRef](#)]
175. Tan, F.; Cong, L.; Li, X.; Zhao, Q.; Zhao, H.; Quan, X.; Chen, J. An electrochemical sensor based on molecularly imprinted polypyrrole/graphene quantum dots composite for detection of bisphenol A in water samples. *Sens. Actuators B Chem.* **2016**, *233*, 599–606. [[CrossRef](#)]
176. Ganganboina, A.B.; Doong, R.A. Functionalized N-doped graphene quantum dots for electrochemical determination of cholesterol through host-guest inclusion. *Microchim. Acta* **2018**, *185*, 562. [[CrossRef](#)]
177. Arvand, M.; Hemmati, S. Analytical methodology for the electro-catalytic determination of estradiol and progesterone based on graphene quantum dots and poly(sulfosalicylic acid) co-modified electrode. *Talanta* **2017**, *174*, 243–255. [[CrossRef](#)] [[PubMed](#)]
178. Arvand, M.; Hemmati, S. Magnetic nanoparticles embedded with graphene quantum dots and multiwalled carbon nanotubes as a sensing platform for electrochemical detection of progesterone. *Sens. Actuators B Chem.* **2017**, *238*, 346–356. [[CrossRef](#)]
179. Wang, Q.; Qin, X.; Geng, L.; Wang, Y. Label-free electrochemical aptasensor for sensitive detection of malachite green based on au nanoparticle/graphene quantum dots/tungsten disulfide nanocomposites. *Nanomaterials* **2019**, *9*, 229. [[CrossRef](#)]
180. Rao, H.; Zhao, X.; Liu, X.; Zhong, J.; Zhang, Z.; Zou, P.; Jiang, Y.; Wang, X.; Wang, Y. A novel molecularly imprinted electrochemical sensor based on graphene quantum dots coated on hollow nickel nanospheres with high sensitivity and selectivity for the rapid determination of bisphenol S. *Biosens. Bioelectron.* **2018**, *100*, 341–347. [[CrossRef](#)]
181. Mirzaie, A.; Hasanzadeh, M.; Jouyban, A. Cross-linked chitosan/thiolated graphene quantum dots as a biocompatible polysaccharide towards aptamer immobilization. *Int. J. Biol. Macromol.* **2019**, *123*, 1091–1105. [[CrossRef](#)] [[PubMed](#)]
182. Santos, A.M.; Wong, A.; Prado, T.M.; Fava, E.L.; Fatibello-Filho, O.; Sotomayor, M.D.P.T.; Moraes, F.C. Voltammetric determination of ethinylestradiol using screen-printed electrode modified with functionalized graphene, graphene quantum dots and magnetic nanoparticles coated with molecularly imprinted polymers. *Talanta* **2021**, *224*, 121804. [[CrossRef](#)] [[PubMed](#)]
183. Axin Liang, A.; Huipeng Hou, B.; Shanshan Tang, C.; Liquan Sun, D.; Aiqin Luo, E. An advanced molecularly imprinted electrochemical sensor for the highly sensitive and selective detection and determination of Human IgG. *Bioelectrochemistry* **2021**, *137*, 107671. [[CrossRef](#)]
184. Ghiasi, T.; Ahmadi, S.; Ahmadi, E.; Babil Olyai, M.R.T.; Khodadadi, Z. Novel electrochemical sensor based on modified glassy carbon electrode with graphene quantum dots, chitosan and nickel molybdate nanocomposites for diazinon and optimal design by the Taguchi method. *Microchem. J.* **2021**, *160*, 105628. [[CrossRef](#)]

185. Anusha, T.; Bhavani, K.S.; Shanmukha Kumar, J.V.; Brahman, P.K. Synthesis and characterization of novel lanthanum nanoparticles-graphene quantum dots coupled with zeolitic imidazolate framework and its electrochemical sensing application towards vitamin D3 deficiency. *Colloids Surfaces A Physicochem. Eng. Asp.* **2021**, *611*, 125854. [[CrossRef](#)]
186. Wang, L.; Tricard, S.; Yue, P.; Zhao, J.; Fang, J.; Shen, W. Polypyrrole and graphene quantum dots @ Prussian Blue hybrid film on graphite felt electrodes: Application for amperometric determination of l-cysteine. *Biosens. Bioelectron.* **2016**, *77*, 1112–1118. [[CrossRef](#)]
187. Zhao, P.; Ni, M.; Chen, C.; Zhou, Z.; Li, X.; Li, C.; Xie, Y.; Fei, J. Stimuli-enabled switch-like paracetamol electrochemical sensor based on thermosensitive polymer and MWCNTs-GQDs composite nanomaterial. *Nanoscale* **2019**, *11*, 7394–7403. [[CrossRef](#)]
188. Li, Y.; Zhang, W.; Zhang, L.; Li, J.; Su, Z.; Wei, G. Sequence-Designed Peptide Nanofibers Bridged Conjugation of Graphene Quantum Dots with Graphene Oxide for High Performance Electrochemical Hydrogen Peroxide Biosensor. *Adv. Mater. Interfaces* **2017**, *4*, 1600895. [[CrossRef](#)]
189. Chowdhury, A.D.; Takemura, K.; Li, T.C.; Suzuki, T.; Park, E.Y. Electrical pulse-induced electrochemical biosensor for hepatitis E virus detection. *Nat. Commun.* **2019**, *10*, 4–7. [[CrossRef](#)]
190. Wang, Z.; Hu, T.; Liang, R.; Wei, M. Application of Zero-Dimensional Nanomaterials in Biosensing. *Front. Chem.* **2020**, *8*, 320. [[CrossRef](#)] [[PubMed](#)]
191. Wang, H.; Li, R.; Li, Z. Nanohybrid of Co<sub>3</sub>O<sub>4</sub> and histidine-functionalized graphene quantum dots for electrochemical detection of hydroquinone. *Electrochim. Acta* **2017**, *255*, 323–334. [[CrossRef](#)]
192. Hatamluyi, B.; Es'haghi, Z. Electrochemical biosensing platform based on molecularly imprinted polymer reinforced by ZnO-graphene capped quantum dots for 6-mercaptopurine detection. *Electrochim. Acta* **2018**, *283*, 1170–1177. [[CrossRef](#)]
193. Tran, H.V.; Le, T.A.; Giang, B.L.; Piro, B.; Tran, L.D. Silver nanoparticles on graphene quantum dots as nanozyme for efficient H<sub>2</sub>O<sub>2</sub> reduction in a glucose biosensor. *Mater. Res. Express* **2019**, *6*. [[CrossRef](#)]
194. Ashrafi, H.; Hassanpour, S.; Saadati, A.; Hasanzadeh, M.; Ansarin, K.; Ozkan, S.A.; Shadjou, N.; Jouyban, A. Sensitive detection and determination of benzodiazepines using silver nanoparticles-N-GQDs ink modified electrode: A new platform for modern pharmaceutical analysis. *Microchem. J.* **2019**, *145*, 1050–1057. [[CrossRef](#)]
195. Yao, J.; Liu, C.; Liu, L.; Chen, M.; Yang, M. An Electrochemical Sensor for Sensitive Determination of L-cysteine and Its Electrochemical Kinetics on AgNPs/GQDs/GCE Composite Modified Electrode. *J. Electrochem. Soc.* **2018**, *165*, B551–B558. [[CrossRef](#)]
196. Shahdost-fard, F.; Roushani, M. Designing an ultra-sensitive aptasensor based on an AgNPs/thiol-GQD nanocomposite for TNT detection at femtomolar levels using the electrochemical oxidation of Rutin as a redox probe. *Biosens. Bioelectron.* **2017**, *87*, 724–731. [[CrossRef](#)]
197. Ting, S.L.; Ee, S.J.; Ananthanarayanan, A.; Leong, K.C.; Chen, P. Graphene quantum dots functionalized gold nanoparticles for sensitive electrochemical detection of heavy metal ions. *Electrochim. Acta* **2015**, *172*, 7–11. [[CrossRef](#)]
198. Shadjou, N.; Saduoghi, E.; Hasanzadeh, M. Highly sensitive quantification of hydrogen-transmitting coenzyme in physiological pH using silver nanoparticles dispersed on nitrogen doped graphene quantum dots. *Microchem. J.* **2019**, *144*, 383–390. [[CrossRef](#)]
199. Nunes, D.; Pimentel, A.; Goncalves, A.; Pereira, S.; Branquinho, R.; Barquinha, P.; Fortunato, E.; Martins, R. Metal oxide nanostructures for sensor applications. *Semicond. Sci. Technol.* **2019**, *34*, 043001. [[CrossRef](#)]
200. George, J.M.; Antony, A.; Mathew, B. Metal oxide nanoparticles in electrochemical sensing and biosensing: A review. *Microchim. Acta* **2018**, *185*, 358. [[CrossRef](#)] [[PubMed](#)]
201. Noy, A.; Artyukhin, A.B.; Misra, N. Bionanoelectronics with 1D materials. *Mater. Today* **2009**, *12*, 22–31. [[CrossRef](#)]
202. Nikolaou, P.; Valenti, G.; Paolucci, F. Nano-structured materials for the electrochemiluminescence signal enhancement. *Electrochim. Acta* **2021**, *388*, 138586. [[CrossRef](#)]
203. Tian, C.; Wang, L.; Luan, F.; Zhuang, X. An electrochemiluminescence sensor for the detection of prostate protein antigen based on the graphene quantum dots infilled TiO<sub>2</sub> nanotube arrays. *Talanta* **2019**, *191*, 103–108. [[CrossRef](#)]
204. Su, S.; Chen, S.; Fan, C. Recent advances in two-dimensional nanomaterials-based electrochemical sensors for environmental analysis. *Green Energy Environ.* **2018**, *3*, 97–106. [[CrossRef](#)]
205. Su, S.; Chao, J.; Pan, D.; Wang, L.; Fan, C. Electrochemical Sensors Using Two-Dimensional Layered Nanomaterials. *Electroanalysis* **2015**, *27*, 1062–1072. [[CrossRef](#)]
206. Ping, J.; Fan, Z.; Sindoro, M.; Ying, Y.; Zhang, H. Recent Advances in Sensing Applications of Two-Dimensional Transition Metal Dichalcogenide Nanosheets and Their Composites. *Adv. Funct. Mater.* **2017**, *27*, 1605817. [[CrossRef](#)]
207. Yu, C.; Yang, J.; Zhao, C.; Fan, X.; Wang, G.; Qiu, J. Nanohybrids from NiCoAl-LDH coupled with carbon for pseudocapacitors: Understanding the role of nano-structured carbon. *Nanoscale* **2014**, *6*, 3097–3104. [[CrossRef](#)]
208. Sanati, S.; Abazari, R.; Morsali, A. Enhanced electrochemical oxygen and hydrogen evolution reactions using an NU-1000@NiMn-LDHS composite electrode in alkaline electrolyte. *Chem. Commun.* **2020**, *56*, 6652–6655. [[CrossRef](#)] [[PubMed](#)]
209. Du, X.; Jiang, D.; Liu, Q.; Zhu, G.; Mao, H.; Wang, K. Fabrication of graphene oxide decorated with nitrogen-doped graphene quantum dots and its enhanced electrochemiluminescence for ultrasensitive detection of pentachlorophenol. *Analyst* **2015**, *140*, 1253–1259. [[CrossRef](#)] [[PubMed](#)]
210. Ashraf, G.; Asif, M.; Aziz, A.; Dao, A.Q.; Zhang, T.; Iftikhar, T.; Wang, Q.; Liu, H. Facet-energy inspired metal oxide extended hexapods decorated with graphene quantum dots: Sensitive detection of bisphenol A in live cells. *Nanoscale* **2020**, *12*, 9014–9023. [[CrossRef](#)] [[PubMed](#)]

211. Singh, V.V.; Nigam, A.K.; Batra, A.; Boopathi, M.; Singh, B.; Vijayaraghavan, R. Applications of Ionic Liquids in Electrochemical Sensors and Biosensors. *Int. J. Electrochem.* **2012**, *2012*, 165683. [[CrossRef](#)]
212. Wei, D.; Ivaska, A. Applications of ionic liquids in electrochemical sensors. *Anal. Chim. Acta* **2008**, *607*, 126–135. [[CrossRef](#)] [[PubMed](#)]
213. Abo-Hamad, A.; Alsaadi, M.A.; Hayyan, M.; Juneidi, I.; Hashim, M.A. Ionic Liquid-Carbon Nanomaterial Hybrids for Electrochemical Sensor Applications: A Review. *Electrochim. Acta* **2016**, *193*, 321–343. [[CrossRef](#)]
214. Zhou, Y.; Zhao, J.; Li, S.; Guo, M.; Fan, Z. An electrochemical sensor for the detection of: P -nitrophenol based on a cyclodextrin-decorated gold nanoparticle-mesoporous carbon hybrid. *Analyst* **2019**, *144*, 4400–4406. [[CrossRef](#)]
215. Wei, M.; Tian, D.; Liu, S.; Zheng, X.; Duan, S.; Zhou, C.  $\beta$ -Cyclodextrin functionalized graphene material: A novel electrochemical sensor for simultaneous determination of 2-chlorophenol and 3-chlorophenol. *Sens. Actuators B Chem.* **2014**, *195*, 452–458. [[CrossRef](#)]
216. Zhu, G.; Yi, Y.; Chen, J. Recent advances for cyclodextrin-based materials in electrochemical sensing. *TrAC Trends Anal. Chem.* **2016**, *80*, 232–241. [[CrossRef](#)]
217. Dong, S.; Bi, Q.; Qiao, C.; Sun, Y.; Zhang, X.; Lu, X.; Zhao, L. Electrochemical sensor for discrimination tyrosine enantiomers using graphene quantum dots and  $\beta$ -cyclodextrins composites. *Talanta* **2017**, *173*, 94–100. [[CrossRef](#)] [[PubMed](#)]
218. Dong, S.; Bi, Q.; Qiao, J.; Shao, S.; Lu, X. Simultaneous determination of three nitroaniline isomers by  $\beta$ -cyclodextrins ( $\beta$ -CDs) and graphene quantum dots (GQDs) composite modified glassy carbon electrodes. *Int. J. Electrochem. Sci.* **2020**, *15*, 8552–8562. [[CrossRef](#)]
219. Shadjou, R.; Hasanzadeh, M.; Heidar-poor, M.; Shadjou, N. Electrochemical monitoring of aflatoxin M1 in milk samples using silver nanoparticles dispersed on  $\alpha$ -cyclodextrin-GQDs nanocomposite. *J. Mol. Recognit.* **2018**, *31*, e2699. [[CrossRef](#)] [[PubMed](#)]
220. Younis, S.A.; Bhardwaj, N.; Bhardwaj, S.K.; Kim, K.-H.; Deep, A. Rare earth metal-organic frameworks (RE-MOFs): Synthesis, properties, and biomedical applications. *Coord. Chem. Rev.* **2021**, *429*, 213620. [[CrossRef](#)]
221. Zamora-Gálvez, A.; Ait-Lahcen, A.; Mercante, L.A.; Morales-Narváez, E.; Amine, A.; Merkoçi, A. Molecularly Imprinted Polymer-Decorated Magnetite Nanoparticles for Selective Sulfonamide Detection. *Anal. Chem.* **2016**, *88*, 3578–3584. [[CrossRef](#)]
222. Zhou, X.; Gao, X.; Song, F.; Wang, C.; Chu, F.; Wu, S. A sensing approach for dopamine determination by boronic acid-functionalized molecularly imprinted graphene quantum dots composite. *Appl. Surf. Sci.* **2017**, *423*, 810–816. [[CrossRef](#)]
223. Xi, J.; Xie, C.; Zhang, Y.; Wang, L.; Xiao, J.; Duan, X.; Ren, J.; Xiao, F.; Wang, S. Pd Nanoparticles Decorated N-Doped Graphene Quantum Dots@N-Doped Carbon Hollow Nanospheres with High Electrochemical Sensing Performance in Cancer Detection. *ACS Appl. Mater. Interfaces* **2016**, *8*, 22563–22573. [[CrossRef](#)]